Manuscript of the article: András Gergely, Imre Bertóti, Tamás Török, Éva Pfeifer, Erika Kálmán†: Corrosion protection with zinc-rich epoxy paint coatings embedded with various amounts of highly dispersed polypyrrole-deposited alumina monohydrate particles.
Appeared in: Progress in Organic Coatings 76(1): 17-32 (2013)
http://dx.doi.org/10.1016/j.porgcoat.2012.08.005

Corrosion protection with zinc-rich epoxy paint coatings embedded with various amounts of highly dispersed polypyrrole-deposited alumina monohydrate particles

András Gergely [a,*], Imre Bertóti [b], Tamás Török [a], Éva Pfeifer [c], Erika Kálmán [b, †]

[a] Department of Metallurgical and Foundry Engineering, Faculty of Materials Science and Engineering, University of Miskolc, B/1 Building, 3515 Miskolc, Hungary

[b] Institute of Materials and Environmental Chemistry, Research Centre for Natural Sciences, Hungarian Academy of Sciences, Pusztaszeri út 59-67, 1025 Budapest, Hungary

[c] Institute of Molecular Pharmacology, Research Centre for Natural Sciences, Hungarian Academy of Sciences, Pusztaszeri út 59-67, 1025 Budapest, Hungary

ABSTRACT

Active anodic zinc content below 90 wt.% does not support sufficient electrical contacts but higher contents cause high porosity of traditional liquid zinc-rich paints (ZRPs). To resolve this problem, our proposal is the application of highly dispersed polypyrrole (PPy) coated alumina inhibitor particles (PCAIPs) in zinc-rich paint compositions. Using these nano-size inhibitor particles at concentrations from 4.55 to 0.85 wt.%, hybrid paints were formulated with zinc contents ranging from 60 to 85 wt.% at the same time. Submicron morphology and nano-scale structure, spectroscopy characteristics and electrochemical properties of the PCAIPs were studied by transmission electron microscopy (TEM) and rheology, Fourier-transform infrared spectroscopy (FT-IR) and cyclic voltammetry (CV) in first part of the work. In the second part, electrolytic corrosion resistivity of two sets of paint coatings were salt-spray chamber and immersion tested with 5 wt.% aqueous solution of sodium chloride. Active corrosion prevention ability of the salt-spray tested coatings was evaluated in compliance with ISO recommendations. Dielectric properties of the coatings during the immersion tests were monitored by electrochemical impedance spectroscopy (EIS). Corrosion tested area of the coatings was investigated by glow-discharge optical emission spectroscopy (GD-OES) to disclose infiltration of corrosive analytes and oxygen enrichment in the cross-section of the primers in comparison with their pristine states. Morphology of the zinc pigments was examined by scanning electron microscopy (SEM), and quality of steel specimens and the interfacial binder residues by X-ray photoelectron spectroscopy (XPS) as well as FT-Raman and Mössbauer spectroscopy. The results of both types of corrosion tests evidenced efficient utilisation of sacrificial anodic current for galvanic protection and improved barrier profile of the hybrid coatings, along with the PCAIP inhibited moderate self-corrosion of zinc. As a result of well balanced active/passive function, the hybrid coating

*Corresponding author. Tel.: +36 1 4381166 /545, fax: +36 1 4381164. E-mail address: andras.gergely@ttk.mta.hu

† Erika Kálmán deceased so she has not seen final version of the manuscript.

containing zinc at 80 wt.% and PCAIPs at 1.75 wt.% embedding PPy at 0.056 wt.% indicated the most advanced corrosion prevention. Galvanic function of the hybrid paints is interpreted on the basis of size-range effect and spatial distribution of the alumina supported PPy inhibitor particles and basic electrical percolation model considerations.

Keywords: A. cold-rolled steel, polypyrrole; B. XPS, GD-OES; C. cathodic protection, hybrid paints

1. Introduction

Corrosion protection performance of hitherto extensively investigated liquid ZRPs [1,2] is limited by the electrical and electrolytic conductivity of the primer coatings [3,4]. The former is connected to the electrical percolation phenomena relating to the pigment volume concentration (PVC) and the latter is affected by the porosity of the coatings. Porosity determines accessibility of anodic pigments by the electrolyte, affecting electrical conductivity of the primers as well as the intensity of sacrificial and self-corrosion of the zinc. These factors have a strong impact on the effectiveness and durability of active galvanic and passive barrier function of the ZRPs [5]. In these aspects, several ZRP compositions were studied revealing the influence of various size and shape of the pigments [6,7] as well as paint formulations [8]. Combination of the ICPs with sacrificial metallic grains is to retain galvanic function and reduce electrolytic conductivity of the ZRPs in the form of using stand-alone ICPs [9] or composited primers [10]. To amend inefficient mechanical blockage of conventional ZRPs [11] and to improve zinc-rich powder coatings [12], intrinsically conducting polymers (ICPs) have been successfully used as mild inhibitor agents to advance corrosion resistance of hybrid paints over ICP-free coatings. Further development was achieved by physical mixture of organic particles and inorganic pigments, but the idea to attain valuable improvement of galvanic protecting organic coatings relies on the formulation of hybrid paints containing highly dispersed particle supported ICPs along with the active anodic metallic pigments. Dispersity related problems of the ICPs are resolved in the course of coating preparation by following the approach of small carriers supported polymers [13]. These nano-size range particle supported ICPs allow to obtain highly dispersed composites [14-16] with greatly enhanced barrier properties [17,18]. The highly dispersed particles [15,14,19] feature increased conductivity and processibility [20] with improved corrosion protection ability [21]. Owing to the fact that zinc corrosion is effectively inhibited by PPy [22], carrier supported PPy is expected to be a favourite filler in zinc-rich hybrid paints. Although viable inhibition function of the PPy requires its partially oxidized form – doped state with immobile counter ion stabilisation [23], undoped ICPs are generally more favourable in paint applications [24] because of the compatibility with organic binders avoiding dispersability and binder compatibility related issues [25]. Although functionalized carriers can promote stable ICP doping, increased hydrophilicity of the materials remains to be addressed prior to successful anticorrosive paint adoption.

In these aspects, in this work PPy is used as nano-size alumina supported particles which are highly dispersed at submicron-scale in the primers so as to enhance electrical conductivity of the coatings and inhibit the corrosion of the zinc pigments. Although PPy deposited nano-size alumina was solely utilized in composite coatings to protect directly aluminium from corrosion [26], whereas the effects of various types of PPy modified alumina has been studied recently [27], the influence of altered ratio of the inhibitor particles and the sacrificial zinc pigments on the corrosion resistivity of particular hybrid formulations has not yet been disclosed. In an effort to achieve firm and durable corrosion prevention performance at the same time, this work is devoted

to investigate various hybrid formulations in order to gain valuable improvement by certain zinc-rich compositions. Furthermore, the main scope is to find optimal balance between inhibition of sacrificial action of the zinc and galvanic function of the hybrid coatings by altered pigment/particle ratios.

2. Materials and methods

2.1. Synthesis of polypyrrole deposited alumina particles

Fumed alumina (Evonik Industries AG, Germany) was dispersed in aqueous ethanol (50 ml) by vigorous stirring for 1 h. Pyrrole (Aldrich) was dissolved at a concentration of 2×10^{-2} mol dm^{-3} and the suspension stirred for 2 h. Solutions (10 ml) of iron(III) nitrate (Fluka) and nitric acid (1 M) were added stepwise to the mixture stirred at 1800 rpm. The molar ratio of iron/pyrrole was set to 1.28 to gain acceptable polymerization rate, whereas pH of the dispersant was adjusted to 3 to moderate the rate of pyrrole polymerisation and deposition. After that low stirring rate (400 rpm) was applied for 6 h prior to the deposition of PPy. Then, the mixture was let stagnant for 16 h. PCAIPs were obtained by decantation, filtering off the precipitate and washing the solid neutral with water 12 times. Finally, the solid was dried and ground.

2.2. Preparation of paint coatings

Paint coatings were tested on standard, low-carbon cold-rolled steel panels (RS type CRS, complying with ASTM A1008.1010, A-109, and QQS-698 standards, roughness; 25–65 micro-inches) were used as received (Q-Lab Ltd., USA). No particular surface treatment was applied to steel specimens without introducing other methods raising the probability of decreasing repeatability of the corrosion tests.

The PCAIP sample was dispersed in the solution of epoxy dissolved by 80% xylene (Fluka), 10% 1-methoxy-2-propanol (Fluka) and 2-butanon (Aldrich) by 20 min milling. Suspension of the PCAIPs was mixed with component A–stabilised zinc-rich masterbatch (HZO Farbenzinkstaub, Norzinco GmbH) in epoxy (Epoxidharz CHS141, bisphenol-A epoxy resin, Prochema), which was diluted to set final concentration. Component B–poly(amido amine) cross-linking agent (Durepoxy H15VP, USNER) was added to the suspension stirred to homogenise, and diluted to get desired wet-concentration. Primer coatings were roll-blade casted in 90 μm wet thickness (35±5 μm dry thickness) and let cure for a week at room temperature. Primers were top-coated with Macrynal SM 2810/75BAC hydroxyacrylic resin (CYTEC Industries Inc.) which was cured with aliphatic polyisocyanate resin; hexamethylene diisocyanate (Desmodur® N75MPA/X, Bayer MaterialScience LLC) dissolved in n-butyl acetate, xylene and isobutanol (2:2:1) in 120 μm wet thickness including hardened primer (80±5 μm overall dry thickness), let cure for three weeks at 25±3 ^{o}C. Scribes were made by a blade as X-cuts. Composition of the formulated paint coatings are summarised in Table 1.

2.3. Characterisation of polypyrrole deposited alumina particles

2.3.1. Elemental analysis

Elemental analysis was performed by a vario EL *III* micro and macro CHNOS elemental analyzer (Elementar Analysensysteme GmbH, Germany) with about 4 mg of the sample.

2.3.2. Transmission electron microscopy

The PCAIP was crushed under ethanol and deposited onto copper grids which were covered by carbon supporting films. Transmission electron microscopy (TEM) data were acquired with a FEI MORGAGNI 268(D) microscope (FEI Co., The Netherlands) operated at 100 kV, with tungsten filament (top-entry; point-resolution=0.5 nm).

2.3.3. Rheology

Flow behaviour of suspensions and colloid sols is related to the interaction of dispersed particles. In addition, rheology control is sensitive to the extent (concentration and dispersity of solids) and strength of interfacial forces (depending on chemical nature of the filler) between suspended materials, viz. boehmite alumina and PPy-modified alumina, through the lipophile matrix. Therefore, rheology study was performed in organic solution of dissolved alkyd resin to estimate macrostructure of the inhibitor particles and corroborate suggestions made by TEM observations. Dried powder of the PCAIPs was wetted with toluene and swelled for three days. Then the solid was crushed in mortar and dispersed by half an hour grinding in the mixture of *n*-butanol and xylene (7:93) dissolved alkyd resin (SYLVATAL™ 25/30LT type distilled tall oil containing free fatty acids (70%) composed of saturated fatty acids 3%, oleic acid 17%, linoleic acid and other non-conjugated 41% as well as polyunsaturated acids (conjugated components) 9%, free rosin acids 27% and unsaponifiables 3% by weight, supplied by Arizona Chemical, Gersthofen, Germany**)**. Composition of the dispersions is summarised in Table 2. Rheology study was carried out with a HAAKE RheoSress RS1 rotational rheometer (Thermo Fisher Scientific Inc., USA) equipped with a cone/plate (2^o angle, Ø 35 mm) sensor at a temperature range of 25±0.3 ^oC.

2.3.4. Fourier-transform infrared spectroscopy

Fourier-transform infrared (FTIR) spectra of the free-standing forms of PPy and PCAIPs were measured by ATR (Attenuated Total Reflection) technique by the means of a Varian Scimitar 2000 FTIR (Agilent Technologies Inc., USA) spectrometer equipped with a 'Golden Gate' (SPECAC) ATR unit with diamond optical element. 128 scans were co-added with 4 cm^{-1} resolution in the spectral range of 4000–600 cm^{-1}. All spectra were ATR corrected using the Varian ResolutionPro 4.0 software.

2.3.5. Cyclic voltammetry

Three-electrode cell configuration was applied for all electrochemical experiments. A platinum spiral (A≈13 cm^2) and saturated calomel electrode (SCE) were used as counter and reference electrodes. A platinum disc used as working electrode (13 mm Ø) was incorporated in a Teflon tube. Pressed pellets of the PCAIPs were attached to the working electrode fixed by a Teflon bracket and allowed to swell in a 0.1 M acetonitrile solution of sodium perchlorate (Aldrich). PPy contents were reduced at –0.4 V for 30 min, then voltammetry scanning performed at a rate of 10 mV s^{-1}. Such sweep rate was used to avoid capacity fading, electroactivity and reversibility deterioration of PPy during the measurements. Repeatability was assured by mitigating ionic mass

transport limitations. Low amount of the PCAIP was pressed to pellets (~1 mm thickness of ~0.15 g, at a density of 1.13 g cm^{-3} on average) with the pressure of no more than 250 kg cm^{-2}.

2.4. Characterisation of paint coatings

2.4.1. Electrochemical impedance spectroscopy

A platinum spiral, SCE and glass-tube-fitted paint coatings covered steel panels (A=5.3 cm^2) were used as counter, reference and working electrodes. The electrochemical cell and the employed Zahner IM6eX potentiostat–frequency analyser (supplied by Zahner-elektrik GmbH & Co., Germany) were placed in two grounded Faraday cages wired to each other. OCPs were measured in an open cell configuration. Electrochemical impedance spectroscopy (EIS) measurements were carried out in the frequency range of 10 kHz and 20 mHz, applying 20 mV sinusoidal perturbation in accordance with the principles of EIS investigation of high resistance paint coatings [28].

2.4.2. Scanning electron microscopy

Scanning electron microscopy (SEM) observations were carried out using a Zeiss EVO XVP 40 (Carl Zeiss AG, Germany) with settings of EHT=20.00 kV and at WD=8 mm, mounted with an INCAx-sight EDS hardware for detection of secondary and quadrant backscattered electrons.

2.4.3. Glow-discharge optical-emission-spectroscopy

Sample preparation for the radio-frequency glow-discharge optical-emission-spectroscopy (GD-OES) analysis was started with the removal of urethane top coat by gentle polishing, leaving zinc-rich epoxy primer intact in thickness of 40 μm. Elemental depth profiling experiments were carried out using a GD–Profiler 2^{TM} radio-frequency glow-discharge optical emission spectrometer (supplied by HORIBA Jobin Yvon S.A.S., France). Sample area was investigated at constant pressure (500 Pa) under argon atmosphere. For high sensitivity element detection, sputtering was performed at constant power (40 W) with voltage settings for the module (8.5 V) and the phase (3.0 V). Flushing time was 5 s at radio frequency plasma excitation of 13.56 MHz with an anode diameter of 4 mm. Depth profile data are presented over thickness of 60 μm including sputtering depth of 20 μm into the steel specimens.

2.5. Characterisation of immersion tested cold-rolled steel specimens

2.5.1. X–ray photoelectron spectroscopy

Paint coatings on steel panels were removed by 5 min ultrasonication in the mixture of dichloromethane, methanol, toluene and tetrahydrofurane (6:1:1:1) applied for three times. X–ray photoelectron spectroscopy (XPS) spectra were recorded on a Kratos XSAM 800 spectrometer (Kratos Analytical, Great Britain) operated at fixed analyser transmission mode using Mg $K\alpha_{1,2}$ (1253.6 eV) excitation. Pressure of analysis chamber was lower than 1×10^{-7} Pa. Wide scan spectra were recorded in the 100–1300 eV kinetic energy range, applying pass-energy (80 eV) in 0.5 eV steps with 0.5 s dwell time. High-resolution spectra of characteristic photoelectron lines of constituent elements, and the C 1s region for carbon-containing layers were recorded at pass-energy (40 eV) by 0.1 eV steps with 1 s dwell time. Spectra were referenced to the energy of C1s

line of polymeric or hydrocarbon type adventitious carbon, set at 285.0 eV binding energy. Chemical states of constituent elements were determined using literature data [29,30]. Kratos Vision 2000 software was used for quantifications with experimentally determined sensitivity factors.

2.5.2. FT–Raman spectroscopy

Removal of the paint coatings was performed by the same process applied for XPS investigation. Measurements were performed using a FT-Raman spectrometer equipped with a dynamic aligned interferometer (BioRad/Digilab Division, Cambridge, USA) operating with 1064 nm Nd:YAG excitation laser at power of 200 mW with 4 cm^{-1} resolution. Spectra were collected by co-addition of 1024 individual spectra and with white light correction.

2.5.3. Mössbauer spectroscopy

^{57}Fe conversion electron Mössbauer spectroscopy (CEMS) measurement was performed at room temperature on steel surface coated with the immersion tested **H1** paint coating [31], by using a conventional Mössbauer spectrometer (WissEl, Wissenschaftliche Elektronik GmbH, Germany) and a ^{57}Co(Rh) radioactive source. The analysis of the Mössbauer spectrum was performed by the MossWinn program [32].

2.6. Immersion and salt-spray chamber corrosion tests

Immersion tests were carried out in 1 M sodium chloride (Reanal) solution at room temperature for 254 days (6100 h), changing the electrolyte in a 42 day period. Salt mist corrosion tests were performed by a spray/prohesion/humidity cabinet (SF/MP/AB100 (C+W Specialist Equipment Ltd., UK) installed with a Jun-Air oil-free compressor (OF302, Gast Manufacturing, Inc., USA). 45 min cycles were divided into two phases. In the first 25 min, samples were exposed to salt fog at 35 ^{o}C combined with Prohesion®, with a dosage rate of 7 ml min^{-1} of NaCl solution (5 wt.%) at 45±3 ^{o}C. In the second phase, temperature was held at 35 ^{o}C for 20 min. Test cycles were repeated until 142 days (3400 h).

3. Results and discussion

3.1. Characterisation of the polypyrrole deposited alumina particles and their dispersions

TEM images of the PPy coated boehmite alumina (γ-AlOOH) particles are presented in Fig. 1a and b at magnification of 10,000 and 20,000. Fig. 1a depicts the submicron-scale loosely aggregated larger size flocs of the particles, interacting through smaller density of interlinks at micron-scale. At higher magnification, surface of the nano-size alumina was observed to be almost completely covered by the polymer giving an average particle size of about 30 nm. Modification lead to a minor proportion of individually dispersed alumina, PPy coating pointed by arrow A in Fig. 1b. Furthermore, coherent microstructure of the particles is primarily based on the strong association by both bridging (arrow B) and coalescence type aggregation (arrow C). The globularly structured PPy incorporated numerous alumina grains which were found in moderate proportion with the size of not exceeding 50 nm. Such particles were composed of coalescence merged several core-shell type PCAIPs, showing a multiphase structure. However, the higher

magnification image of Fig. 1b reflects clearly on the well dispersed and associated structure of the inhibitor particles. The yield of pyrrole polymerisation and deposition on alumina was determined by the elemental analysis. Carbon and nitrogen were measured at 2.41 wt.% and 0.73 wt.% on average respectively, corresponding to a 3.28 wt.% PPy content which was far lower than the targeted 4.94 wt.% in case of complete polymer deposition. This is attributed to the medium solubilizing strength of the aqueous ethanol solvent (causing residing PPy in bulk solution), allowing less effective anchoring and partial deposition of PPy on the positively charged surface of alumina, despite the high performance chemical process [33] and the preferred iron(III)/pyrrole ratio [34].

In Fig. 2 the IR spectrum of the PCAIP is compared to the spectra of free-standing PPy samples prepared in water (PPy1) and aqueous-ethanol solution **(**PPy2). In the PPy1 spectrum typical bands of polypyrrole are shown at 1528 and 1467 cm^{-1} νC-C and νC=N stretching of the pyrrole ring appear, while the bands at 1285 and 1142 cm^{-1} belong to the C–H deformations [35,36]. The weak, but well defined band observed at 1093 cm^{-1} corresponds to the in plane deformation mode of NH_2^+ formed on PPy chains by protonation [37]. As to the aqueous-ethanol prepared PPy2, a doublet at 1554 and 1531 cm^{-1} in the C-C stretching region appears in the spectrum as a result of a combination of an intra-ring C=C vibration and an inter-ring C–C stretch [35]. Furthermore, the slight blue-shift of all peaks is attributed to a more compact, three-dimensional structure of PPy2. In the case of alumina supported PPy (PCAIP) spectral features are changed. The new bands at 1634 and 1340 cm^{-1} are assigned to the deformations of protonated species, NH_2^+ of doped PPy. The broad, intensive band around 1120 cm^{-1} corresponding to the C–H in-plane deformation vibrations of PPy suggest a compact, three-dimensional structure in the aqueous ethanol-solvent-prepared PCAIPs. The blue-shift of C=C/C–C inter and intra-ring vibration in the spectrum may be explained by an enhanced electron delocalization in the PPy backbone [38].

Cyclic voltammetry indicated moderate redox ability and electroactivity of the PPy. The voltammetry current density of the PCAIP exceeded the double-layer capacitance and adsorption related background current measured by platinum electrode at the same sweep rate. Despite the low current transient, highly reversible current response was obtained with the location of oxidative peak potential at 0 V and low charging efficiency (supplementary data). The low current transient and coulombic efficiency are resulted by the semi-conductivity of undoped PPy and the low polymer contents of the PCAIP. The latter is in correspondence with the onset of electrical percolation threshold found at around 4 wt.% of polymer contents [39].

To obtain complementary microstructure information beyond TEM observation based on interaction of the solid particles, PCAIPs were dispersed in dissolved alkyd binder and studied by basic rheology terms. Interactions between the particles within the dispersion of dissolved vehicle are based on the ability to build up apolar and polar interactions, whereas contribution of hydrogen bonding is secondary. In addition, hydrated alumina is ineffective but PPy modified alumina is in favour of interacting with each other through lipohile matrices. Therefore, dissolved alkyd vehicle was used for dispersion structure investigation (also due to the minimum dispersion stability requirement during the measurements). This is because dispersity and distribution of the particles are slightly affected by this type of organic dispersant change due to the Hansen solubility indexes [40] but properties of the particle dispersion can be more sensitively characterized by using lipohile matrix like alkyd polymer. Otherwise, solid particle concentration of 3.846 wt% was set to a particle content range valid in epoxy resin of the cured **H1–H5** hybrid paints. The presumption of three-dimensional distribution of the inhibitor particles in the organic resin is relevant to interpret the corrosion resistivity of the hybrid coatings. Dynamic measurement results are

presented in Fig. 3a and b. As it is reflected by the unchanged complex viscosity (Fig. 3a), the wide frequency range linear ramps of the storage and loss moduli associated with rapid relaxation processes reflect Newtonian flow of the dissolved alkyd vehicle and its dispersion with bare alumina hydrate. In both cases, the higher loss and lower storage moduli indicate viscous flow characteristic in accordance with the absence of association of dispersed alumina and the lack of coherent microstructure of the colloid sol. Nevertheless, high surface/volume ratio, dispersity of the alumina is accounted for the increased dynamic viscosity as a result of notable volume exclusion of the nano-size filler. As it is expected, constant storage and loss moduli with high loss factor vs. applied stress measured in amplitude sweep mode (Fig. 3b) confirm the suggestions made based on the results of frequency sweep test.

Dispersion of the PCAIP exhibited completely different behaviour. The higher storage and the lower loss moduli indicated in Fig. 3a confirm a viscoelastic response featuring pseudo-solid like behaviour which is associated with a medium spatial density interlinked, coherent microstructure of the sol. The elastic-viscous transition with intersecting storage and loss moduli at ~4 Hz suggests moderate stress-activation related deterioration of the three-dimensionally highly associated colloid system. The steeply increasing loss factor indicates quasi-solid and viscous transition. Vast increase in the complex viscosity compared to the alumina dispersion is connected to the enhanced inter-particle interactions of the highly dispersed filler phase. The greater interfacial attractive forces through dissolved alkyd matrix are connected to the small quantity of PPy content of the PCAIPs as a result of preferred interfacial interactions between the lipohile matrix and the particles based on the match of solubility parameters of pyrrole ($\delta_{D,P,H}$=19.2,7.4,6.7) and phenolic species (18,5.9,14.9) [40]. The lack of effective hydrogen bonding between alumina and the dispersant leads to an inefficient enthalpy gain over the negative entropy effect. Hence, hydrated alumina repels much of the alkyd matrix, since insignificant rheology control of alumina is connected to the weak van der Waals forces between the solid and the vehicle. On the other hand, enhanced interfacial attractive forces between the liquid phase and the highly dispersed PCAIPs are responsible for the higher mobility restriction of alkyd polymer segments and the effective load transfer related massive flow resistance. The observed plateau in the loss factor between 10 and 100 Hz supports the notion of high strain rate yielded deterioration in the colloid structure. As it is presented in Fig. 3b, amplitude sweep measurement reveals two-stages of stress-activated attrition of the macro and micro-gel structure of the PCAIP dispersion with elastic-viscous transition signified by intersecting storage and loss moduli at 10 Pa. The former is attributed to the less extensively interlinked three-dimensional floc system and moderate association of the particles within the micro-gel flocs. The latter is connected to the stress amplitude (critical stress level) induced collapse of the coherent pseudo-solid like gel system. Decreasing complex viscosity points out effective shear-induced reorientation, disruption of the three-dimensionally association.

Constant rate measurement results are shown in Fig. 3c. The small hysteresis loop and the low monotonic shear-thinning is a result of insignificant structural viscosity of dissolved alkyd matrix. Similar flow behaviour of the alumina dispersion is indicated by Newtonian plateau of the apparent dynamic viscosity over wide strain rate. Hence, this sheds light on the microstructure of the sol composed of randomly distributed particles, featuring hydrodynamic control of the freely moving particles during stress activated macroscopic flow. In the case of PCAIP dispersion, the various strength and scale of particle association and rearrangement are reflected by the highest strain rate related large hysteresis as well as the different slope of shear-thinning effect. The all strain rate higher forward (fw.) than backward (bw.) apparent dynamic viscosity leading to considerable thixotropy index of the PCAIP dispersion mean moderate reorientation rate of the

particles and slower recovery of the colloid structure. Along with the large thixotropy, continuous shear-thinning is associated with increasing deterioration and disruption of the interlinked flocs with subsequent gradual floc attrition – activation of bridging flocculated and coalescence aggregated particles. Nonetheless, all kinds of interparticle attractive interactions diminish by continuous straining at high strain rates, leading to complete disruption of the micro-gel flocs. This is indicated by the same hydrodynamic flow resistances of the alumina and the PCAIP dispersions measured at a rate of $300\ s^{-1}$ (Fig. 3c). In addition, the high yield-stress (Fig. 3d) supports the suggestion of highly interlinked floc system – interacted microstructure of the well dispersed inhibitor particles (featuring high effective volume fraction).

3.2. Investigation of paint coatings

3.2.1. Immersion test monitored with open-circuit potential and electrochemical impedance spectroscopy

OCPs and impedance data of the immersion tested neat epoxy (**E**), alumina contained zinc-rich **ZA** and the conventional type zinc-rich **Z** paint coatings covered steel samples are presented in Fig. 4a and b-d. In the case of neat epoxy coated steel sample, the strong anodically shifted and fluctuated OCPs (Fig. 4a) suggest very low rate of interfacial redox processes up to the 152 days of immersion. The largely hindered, slow water uptake of the coating is confirmed by the durable and massive electrolytic resistance – high impedance, which unanimously reflected by the almost ideal capacitive behaviour, the absence of dipolar and ionic of the coating signed by the high low-frequency impedance amplitude and low phase-angle minimum without a sign of breakpoint or saddle frequency in the phase spectra (Fig. 4b). Hence, as it is expected, firm and stable passive protection by the **E** is recognised. However, the effect of slow electrolyte infiltration was experienced after 175 days by the lowly increasing low-frequency phase-angle minimum and the stabilizing OCPs. Positive polarised mixed potential supports the idea of shrinkage in the area of anodic processes, evidencing suppressed iron dissolution processes. At 225 days, the extent of anodic polarisation decreased which must be the result of increasing rate of anodic processes at the steel surface.

For the traditional type zinc-rich **Z**, mixed potentials remained between –0.9 and –1.0 V vs. SCE over 127 days (Fig. 4a) which means long-term stable and effective cathodic polarisation – thermodynamic immunisation of steel substrate against corrosion. This was allowed by the high porosity of the primer and the intense anodic action of the zinc pigments. In the meantime, as it is explained by the impedance data exhibited in Fig. 4c, low barrier nature of the **Z** is confirmed by the small and decreasing impedance amplitudes as well as the low low-frequency phase-angle minimum along with the high-frequency domain shifted breakpoint frequencies. This is the consequence of high porosity of the high PVC featured primer. Drops in the impedance moduli at 38 and 172 days correlated with the corrosion products blocked electrolyte infiltration – deactivation and the greater electrolyte ingress caused reactivation of galvanic function of the primer. Around 73 and 200 days, these terms were followed by less effective evolution and moderate recovery in the mechanical blockage driven by altered rate of accumulation and dissolution of zinc corrosion products. The observed second time constant in the phase diagram between 127 and 200 days is a result of increasing double layer capacitance and interfacial redox processes with an inherent implication of minor corrosion of the substrate. Intense sacrificial and self-corrosion of part of the zinc pigments was appointed in the **Z** by cross-sectional SEM observations (supplementary data), finding a great deal of corroded phase at a considerable

proportion of the grain boundaries. High porosity led to enhanced sacrificial corrosion of zinc, allowing high rate of ORRs and the evolution of strongly alkaline milieu. Despite severe delamination of the **Z**, which is in accordance with oxidative degradation [41,42] and saponification of the epoxy binder, no corroded spots was detected on the steel surface.

The completely opposite case was ascertained to the alumina contained zinc-rich **ZA**. During the first 40 days, OCPs became slightly cathodic (Fig. 4a) and the nearly same kind of impedance data (Fig. 4d) suggested unchanged electrolytic conductivity of the coating. However, within the next 35 days of immersion, cathodically polarised potentials coincided with the considerable drop of the low-frequency impedance amplitudes and increased phase-angle minimum with the higher frequency range measured breakpoint frequency. These are all support the notion of greater electrolyte infiltration – activation of the primer with deteriorated, ineffective barrier behaviour of the coating. Then, steadily decreasing OCPs and the migration of breakpoint and saddle frequencies into the low frequency domain reflect insignificant porosity decreasing influence of the accumulated corrosion products on the rate of electrolyte ingress. Therefore, the cathodically polarised and stabilised potentials with the character of impedance profile suggest inefficient galvanic function and undergoing anodic processes in the coating/steel interface to some extent. The following term signified by the stable cathodic OCPs around –0.6 V vs. SCE with gradual shift of the breakpoint and saddle frequencies towards the higher frequency range is connected to low rate of steel corrosion with continuous further decrease in the passive protection ability. At the end of the test, steel substrate was moderately corroded and the coating was considerably blistered and slightly delaminated. The overall quality appraisal is included in Table 3. Consequently, paint coatings based on the composition of highly dispersed alumina hydrate and spherical zinc at contents of 3.21 and 70 wt% provides neither efficient galvanic nor firm barrier protective function to steel substrates.

OCPs and impedance data of the immersion tested hybrid paint coatings are presented in Figs. 5a and b-f. Anodically shifted OCPs (Fig. 5a) indicate the initial phase of electrolyte infiltration related activation of the **H1** coating taking place within 10 days. Although OCPs shifted altogether more than –0.4 V into the less cathodic polarisation range in the initial 33 day period, stable barrier function of the **H1** is noted by the impedance data of unchanged low-frequency impedance moduli with nearly the same profile of phase-angle spectra characterised by the breakpoint and saddle frequencies (Fig. 5b). Hence, this term is recognised as more efficient passive but less viable active corrosion protection function. This behaviour changed a lot around 50 days of immersion when OCPs stabilised at –0.4 V and impedance data showed greater electrolytic conductivity by decreasing low-frequency impedance modulus. To the end of this term at 127 days, the emerge of a second time-constant in the phase spectra is attributed to the increased higher rate of interfacial corrosion processes accompanied with increased double-layer capacitance associating with higher amount of corrosive electrolyte at the steel surface. Durable anodically polarised OCPs with quite similar impedance data measured until 172 days hint on the somewhat stabilized barrier nature of the coating. This should be the consequence of low coating porosity and the 4.55 wt.% inhibitor particle allowed low intensity sacrificial action of the zinc with the accumulation of small amount of corrosion products. Although the before mentioned procedures did not resulted in remarkable recovery in barrier function of the **H1**, the long-term low intensity galvanic function of the hybrid primer led to diminish increased rate of corrosion processes in the coating/steel interface and higher efficacy barrier nature. These are indicated by the disappeared second time-constant at 0.1 Hz in the phase spectra as well as the same magnitude impedance amplitudes in the Bode plot. As a result of interfacial corrosion processes, **H1** delaminated completely from the substrate but the surface of steel panel was almost free of corrosion (see XPS and Mössbauer results).

The lower amount of PCAIP contained **H2** hybrid paint with the same zinc PVC exhibited altered protection function. Longer electrolyte ingress related induction time was noted with stable passive character by the anodically polarised OCPs (until 20 days) measured with decreasing impedance moduli and increasing low-frequency phase-angle minimum (Fig. 5c). The **H2** hybrid containing lower amount of PCAIPs (3.67 wt.% compared to that of **H1**) exhibited short-term cathodic polarisation of the OCPs around 30 days, which is connected to more intense anodic action of the zinc and the related galvanic function of the primer. At 61 days of immersion, mixed potential became strongly anodic and the phase-angle data of the impedance results revealed ether diffusion or rather porous diffusion kinetic regime (phase-angle between -45^{o} and -20^{o} over wide frequency domain) through the coating, hinting on the increasing efficiency of barrier properties. Then, cathodically shift of the potentials from 127 to 175 days was accompanied by herewith effective evolution of the barrier nature signified by the high impedance moduli and the low-frequency range migrated breakpoint frequency. In the last 50 days of the test, changes in the impedance data are connected to the gradually deteriorating barrier properties. Nonetheless, greater efficiency of galvanic function of the **H2** hybrid formulation is reflected by the absence of blistering and delamination of the coating as well as rust-free condition of the steel substrate after the 254 days time period.

The hybrid paint formulation based on the composition of 70 wt.% zinc and 3.21 wt.% PCAIPs in **H3** afforded some of the lowest intensity but definitely the highest barrier and efficient galvanic protection to the substrate. Even in the initial 30 days, the remarkable anodic shift of the OCPs measured with the high impedance (Fig. 5d) suggest strong barrier capability and significant shrinkage in the area of anodic action of the zinc with the associated very low intensity of galvanic function of the primer. The term of greater electrolyte infiltration caused activation of the **H3** and the zinc pigments with slightly intensifying galvanic action of the primer which proved to be markedly prolonged. Then, the result of slow accumulation rate of corrosion products is signified by the firm anodic polarisation of the OCP and its stabilisation at ~ –0.4 V. This means even more notable decrease in the anodic sacrificial areas and the intensity of zinc dissolution. The evolved barrier nature at 127 days with an almost ideal capacitive character of the **H3** over the 175-214 day period defined by the impedance data are connected to a massively hindered electrolyte diffusion into the coating and to the steel surface. Such an exceptionally firm and stable passive corrosion performance of the **H3** primer seemed to start deteriorate from 230 days when OCPs turned to cathodic and the impedance moduli decreased with increasing low-frequency phase-angle minimum. Reflecting the robust protection performance of this hybrid formulation, no coating delamination, blistering and steel rusting were experienced.

The 80 wt.% pigment cemented **H4** paint (containing PCAIPs at 1.75 wt.%) afforded firm and stable with different protection characteristics compared to the **H3**, which are partly exhibited by the altered OCP and impedance changes as a function of time. Except from small fluctuations, the tendency of OCP changes with gradual anodic polarisation means suppressed galvanic function of the **H4** with less intense contribution of the zinc anodic areas to the mixed potentials obviously because of the continuous decrease in the active surface. Impedance data (Fig. 5e) reveal slow activation of the firm barrier nature featuring **H4** at 73 days by the increased low-frequency phase-angle. This was followed by similar phase-angle changes indicating smaller barrier recoveries at 172 and 254 days and greater electrolyte ingress caused enhanced activation of the **H4** at 200 days. OCPs and the impedance data suggest delicate changes in the active/passive preventive function of the coating. In comparison with the **H3**, more frequent activation of the zinc and recovery of the coating barrier behaviour resulted probably by the accumulation of smaller amount of pore-filling species. However, moderate intensity and efficiency of galvanic function of the hybrid is surmised

based on the fact that the coating completely delaminated but the substrate was free of corrosion. The experienced cathodic delamination phenomenon is in agreement with the intense ORRs taking place at the steel surface under the effective barrier coating assured electrolyte short condition.

Reflecting on the impact of highly dispersed PCAIPs on the active corrosion prevention ability of zinc-rich compositions, inhibited zinc corrosion with the associated suppressed galvanic function of the **H5** primer is pointed by the markedly anodically polarised OCPs of around –0.2 V (Fig. 5a) during the initial 25 days of immersion (in comparison with the conventional type zinc-rich **Z**, Fig. 4a). Such a low intensity (and efficiency) active protection was obtained despite the 85 wt.% zinc content of the coating and the impedance data confirmed firm barrier ability within the initial stage of immersion propagation (Fig. 5f). It is emphasised that without the use of nano-sized inhibitor particles, pure ZRP coatings should have provided viable thermodynamic immunisation to steel substrates against corrosion (–0.86 V vs. RHE) [43], according to our experimental results with series of ZRPs and the finding of S. Shreepathi et al. [1]. Cathodic polarisation of the mixed potentials at 38 days coincided with increased rate of electrolyte infiltration signified by the remarkable drop in the low-frequency impedance amplitude and high-frequency domain migration of the breakpoint and saddle frequencies. At such a high zinc PVC with moderate electrolytic conductivity of the coating, stabilisation of the OCPs between –0.4 and –0.6 V vs. SCE as a result of galvanic coupled system of zinc-rich primer with steel substrate well obviously means low efficacy of active corrosion protection by galvanic currents. The frequent and smaller impedance character changes at 73 and 200 days with the long-term activation by enhanced electrolyte ingress (within the time-frame of 73-200 days) suggest less effective and stable barrier recovery of the coating based on this hybrid formulation. The OCPs of around –0.6 V measured over the last phase of the test up to 254 days are associated with slow rate of iron dissolution – steel corrosion. High intensity and low efficiency galvanic function of the **H5** primer are confirmed by the slightly blistered but completely delaminated coating as well as low density areas of iron rust formation on the steel surface.

Paint formulations with physical mixtures of stand-alone PPy and zinc pigments afforded poor protection, observing various density and extent of corroded spots on the steel surface and severe delamination of the coatings at the end of immersion tests. These are in relation with the low efficacy of galvanic protection ability as well as barrier nature of the primers. The moderately cathodically polarised OCPs obtained for the stand-alone PPy loaded primers coated steel panels were accompanied by high ionic conductivity, leading to considerable coating delamination and steel rusting. On the other hand, highly dispersed PCAIP loaded primer provided efficient anodic protection to the substrate with appreciable effectiveness and long-term stable mechanical blockage. Despite its moderate delamination, tested steel surface was free of macroscopic corrosion spots.

3.2.2. Glow-discharge optical-emission-spectroscopy investigation of immersion tested coatings

Some coating samples were investigated by this technique because of the ability to detect elements in ppm quantities. Relative quantities of coating components and the corrosive species normalized to the intensity of the sum of carbon are presented as a function of sputtered depth. The EIS suggested low electrolytic conductivity and ionic permeability of the highly dispersed alumina comprised zinc-rich **ZA** was affirmed by detection of unchanged quantities of corrosive species in the entire cross-section of the primer, as it is exhibited by the comparison of intensities of the elements in Figs. 6a and b obtained before and after the salt solution test. Aside from the quite similar sum of the anions, 6% increment in the oxygen content in the galvanic coupled half-section

of primer near the steel surface support the idea of moderate barrier ability as well as low efficacy of intense sacrificial and self-corrosion of the zinc with the related inefficient galvanic function of the primer. This must have resulted by the lack of valuable inhibition of the sacrificial pigments which was well available to the hybrid paints loaded with PCAIPs.

The greater amount of inhibitor particles comprised **H2** showed considerable enrichment of potassium within the whole cross-section of the primer (Fig. 7a and b). Although concentration of potassium in the epoxy vehicle is estimated to reach a concentration of around 1 mol dm^{-3} after the corrosion test, the contents of lithium and sodium was almost unchanged. Furthermore, change in the chloride content was around the fluctuation degree of analytes. Thus, the coating featuring such type of hybrid formulation should have maintained low intensity of galvanic function. This was probably contributed by the electrical conductivity of the PCAIPs because ZRPs with spherical zinc content of 60 wt% are clearly unable to provide anodic current based galvanic protection [1,5-7]. Moreover, the intensity of oxygen was found nearly the same in comparison with its ratio to the distribution of zinc and the depth-profile content of carbon. Therefore, **H2** highly likely can afford only limited passive protection ability, hereby confirming the results of EIS investigation. On the other hand, due to the insignificant increase in the oxygen content the coating must have provided low intensity galvanic protection, which is in agreement with the anodically polarised OCPs and XPS analysis (see later). This was resulted by the increased relative amount of the PCAIPs to the quantity of zinc pigments.

Compared to the initial amount of all corrosive analytes like lithium, sodium, potassium and chlorine, these species were detected at almost the same quantities in the cross-section of **H3** after the test indicated by the depth profiles in Fig. 8a and b. This finding corroborates the suggestion of highly hindered electrolyte infiltration into the **H3** based on EIS data. Nevertheless, sodium and potassium were detected in somewhat greater quantities in the half-depth cross-section of **H3** next to its solution interface after the test. As a consequence low electrolyte ingress, corrosive analytes like sodium and potassium accumulated in the epoxy at concentrations of 1.8×10^{-3} mol dm^{-3} and 9.4×10^{-2} mol dm^{-3}, respectively. However, the unchanged chlorine content suggests very limited permeability of the primer to anionic species, shedding light on the low impact of the PCAIPs on electrolytic conductivity and the corrosion prevention function of such type of hybrid formulation. In addition, detection of potassium in the half-depth near the solution interface is due to its smaller hydrodynamic radius allowed higher mobility, faster diffusion and migration in the organic paint coatings [44]. Furthermore, small increase in the oxygen content of the primer near the steel surface (~20–40 μm) and the accumulation of cationic species in the 0–20 μm depth-range hint on the viable cathodic – galvanic function of the hybrid. Detected quality and intensity of elements completed with SEM observations in the cross-section of the **H3** confirmed nearly intact morphology of the pigments and the absence of emerged phase at grain boundaries (Supplementary data). This is in line with XPS results of inhibited anodic action of zinc and low rate of accumulation of its corrosion products.

3.3. Characterisation of steel specimens covered with immersion tested paint coatings

3.3.1. X–ray photoelectron spectroscopy

Due to the amount and ratio of functional groups in the cross-linked and hardened epoxy, concentration of the carboxyl groups was ~2 at.% in the cured primer along with the main components of ether and carbonyl species. Relative content of the highest oxidised state of carbon bonded oxygen species serves as a measure to appraise oxidative degradation of the organic

vehicle in the zinc-rich coatings as a result of various intensities of galvanic function of the primer relating directly to the interfacial electron transfer reactions and ORRs. XPS detected iron and zinc regions acquired from the surface of immersion tested steel panels are presented in Fig. 9a and b. Although absolute peak intensities of iron and zinc are proportional with the amount of interfacial corrosion species, their relative contents (exhibited in Fig. 10) are considered to be more adequate for qualitative analysis. The ratio of zinc oxide/hydroxide hints on the intensity of galvanic function of the primers. The figure displayed data indicate that interfacial accumulation of zinc corrosion products is the highest in the **Z** and decreasing quantities in the **H5** and **ZA**. The lowest relative amount of corroded zinc support the idea of almost an order magnitude lower rate of zinc corrosion within the **H1** compared to the conventional type **Z**. The **H2**, **H3** and **H4** samples showed similarly low rate of zinc corrosion in the galvanic coupled coating/steel interfacial region, agreeing well with the presumptions drawn based on OCP, impedance and GD-OES investigations. High porosity of the **Z** and the lack of valuable inhibition of zinc corrosion in the **ZA** despite its low porosity lead to more intense galvanic function of the primers. Medium degree of coating porosity and the low concentration of the PCAIPs allowed the function of high galvanic activity in the **H5**. The firm barrier nature of the **H2**, **H3** and **H4** with available zinc corrosion inhibition (afforded by the PCAIPs) led to quite low sacrificial action of the metallic pigments. In spite of the moderate barrier ability of the **H1**, which was due to the high PCAIP content caused enhanced electrolytic conductivity, the lowest amount of interfacial zinc corrosion products was ascertained which is obviously attributed to the effective inhibition function of the highest quantity of incorporated inhibitor particles. The carbon normalised quantity of white zinc rust – corroded porous film on the metallic grains with some precipitates on the steel surface suggest that the highest intensity sacrificial function of zinc took place in the **ZA** and the lowest in **H4**. The medium relative amount of zinc hydroxide accumulation in other hybrid coatings may allow us to conclude about moderate degree of sacrificial action of the zinc. Furthermore, relatively small area of the zinc grains became corroded and covered by porous layer allowing further corrosion of the metallic phase of the pigments in the **Z**. Nevertheless, the zinc hydroxide associated galvanic action must have taken place at the highest rate within the interfacial region of the **H2** and **H3** because of the lower zinc PVC compared to other coatings. The ratio of absolute contents of zinc hydroxide and zinc oxide reveals another aspect of zinc corrosion. The high intensities obtained for the **H1**, **H2** and **H3** suggest high rate of zinc corrosion concentrated on smaller area of the grain surface because of the lower pigment contents and the PCAIP caused partially blocked anodic dissolution. Furthermore, quite low rate was found to be valid in the **Z** and the lowest in the **H4**. Therefore, zinc pigments in the **Z** could be somewhat passivated long-term similarly in the **H4** hybrid sample, which is in line with the tendencies of gradual anodic polarisation of the resultant mixed potentials, i.e. OCPs. The latter hints on the continuously decreasing intensity of zinc dissolution. In addition, considering the measured anodically polarised OCPs with the significance of various extents of shrinkages in the active anodic areas, the increased rate of sacrificial function at decreased pigment surface means that much of the PCAIPs took part in the inhibition of zinc corrosion and supported the electrical conductivity – galvanic function (and its efficacy) of the hybrid coatings at the same time, especially in the case of the **H3** and **H4** hybrids. The ratio of corroded species of zinc and iron reveals utilisation efficacy of the anodic current for steel protection. Regarding the extent of corrosion of the zinc pigments and steel substrates, these data support the suggestion that high efficiency galvanic protection was maintained by the **H1**, **H2** and **H3**, whereas much worse utilisations were provided by the zinc-rich primer system of the **ZA** and the **H5** (with the respect of visually easily detectable iron rust on the panels). This result signifies the fact that PCAIPs must have contributed to the electrical coupling between the zinc pigments

and steel substrates because below the percolation threshold [5] durable active steel protection would not have been attained. Insignificant but definitely sensible was the changes in the ratio of iron and the sum of corroded iron species. As presented data show it, the lowest proportion of the superficial iron atoms became corroded and the highest oxidative conversion occurred in the **ZA**. This result is in agreement with the intense and viable galvanic function of the **Z** as well as the poor active protection capability of the **ZA** composition having highly dispersed, non-conductive and hydrophilic nano-size particles around the isolated isotropic zinc pigments. In this range, the ratios of metallic and corroded iron detected on the surface of steel substrates exhibited small increase with the growing zinc contents of the hybrid primers. Hence, greater proportion of zinc and the inhibitor particles resulted in increased galvanic function with remarkable efficacy by the **H2**, **H3** and **H4**, keeping iron of the substrates in metallic state more effectively along with the low rate of zinc corrosion. However, by the comparison of corroded iron species to the sum of carbon, the highest ratio was ascertained to the **H2** sample. This means that decreasing anodic pigment content in the hybrids lead to lower intensity of anodic currents and decreasing effectiveness of the cathodic corrosion preventing function of the zinc-rich systems. High carboxyl conversion of carbon of the epoxy in the **Z**, **ZA** and **H5** is connected to the intense galvanic function caused enhanced interfacial electron transfer reactions and high rate of ORRs. Nonetheless, considering other parameters, these ratios shed light on deteriorated utilisation efficacy of the sacrificially generated anodic currents to the corrosion prevention of steel substrates. Various scales of delamination of the coatings are explained by the oxidative degradation of the organic binder. Nevertheless, similar corrosion degree of epoxy in other hybrids may well support the suggestion of additional protection function of the PCAIPs, involving scavenging oxidative radicals [46] and nucleophile species [47-49] obviating high rate of oxidative degradation of the organic matrix. Thus, less alkaline milieu probably resulted in slower removal of precipitated corrosion products on the surface of metallic grains since inhibited anodic function of the zinc pigments is also connected to their slower reactivation.

3.3.2. FT-Raman and Mössbauer spectroscopy

FT-Raman spectrum obtained from the steel surface coated with the immersion tested **H1** hybrid is presented in Fig. 11a. The band at 1081 cm^{-1} of surface hydroxyl species together with the very small bands at 758, 618, 543, 347 and 119 cm^{-1} in the FT-Raman spectra can be associated with low crystalline type goethite phase (α-FeOOH) [49] on the surface of slightly corroded steel substrate. Nevertheless, the corroded phase was probably not coherent or continues thin film rather it should form island-like spots on the surface, owing to the low intensity signal gain and signal-to-noise ratio. The band at 543 cm^{-1} can be related to some small quantity of magnetite [50] and the bands at 350 and 500 cm^{-1} are assigned as small quantity of maghemite. The bands at 622 and 1320 cm^{-1} and above are connected to the traces of hematite which should be a contaminant phase. The obvious absence of lepidocrocite phase [51] corroborates to presume low rate of hydration and hindered process of chloride induced steel corrosion underneath the **H1**. The low Raman intensity bands are in line with the outcome of XPS analysis, suggesting the mixture of oxidised iron phases, if it is a film within the thickness of 10 nm.

The herewith described result is corroborated by the corresponding ^{57}Fe conversion electron Mössbauer spectrum depicted by Fig 11b. The figure displays one sextet component with ^{57}Fe Mössbauer parameters (zero quadrupole splitting, hyperfine magnetic field of $B_{hf} = 32.82(4)$ T, ^{57}Fe isomer shift of $\delta = -0.007(5)$ mm s^{-1} relative to body-centred cubic iron at room temperature) that characterize the non-corroded steel substrate. The upper limit of the relative area fraction of

non-apparent spectral components is estimated to be below 10% due to the well crystallized oxide phases. This would correspond to an average oxide layer thickness of ~10 μg cm^{-2} [33] being equivalent to an iron oxide layer of around 20 nm in depth. It is highly obvious that such type of thin layer of corroded iron oxide phase evolved under atmospheric conditions before the corrosion tests. Thus, XPS and Mössbauer spectroscopy consistently confirm very low corrosion rate of the steel substrate which owes to the viable corrosion prevention by the hybrid coating.

3.4. Salt-spray chamber test

Despite the long-term and harsh salt-mist propagation, no deterioration and differentiation in the quality of most of the coatings were noticed at 92 days. Carrying out the chamber test for 142 days, corrosion prevention ability measured by steel rusting, blistering and delamination of the coatings could be well defined. Evaluation results are summarised in Table 4, whereas photographs of the samples are presented in Fig. 12 with gradual appraisal over the 142 day period highlighted in Fig. 13. Although the slightly blistered **ZA** at the buried surface would suggest firm passive protection capability, the intense iron rust formation and severe delamination of the coating around scribed areas (Fig. 12) reveal low galvanic efficiency with the associated poor active corrosion prevention. Gradual deterioration of the coating and the continuous rust formation expressed by a unified index (Fig. 13) also support the idea of absence any valuable active protection. The pure zinc-rich **Z** indicated firm resistance against blistering and viable corrosion prevention o steel at the scratched areas. However, it was not able provide acceptable degree of protection over the intact surface against rusting and the osmosis driven blistering. This is the consequence of high porosity and electrolytic conductivity allowed increased rate of coating deterioration proceeding partly via accumulation and subsequent leaching of the massive amount of corrosion products. Such type of degradation of the coating is reflected by the usual switch between deterioration and stabilisation accelerated after 40 days of the test.

The **H1** exhibited intense rust formation around scribes, evidencing only moderate protection functionality by less intensive delamination and blistering over the activated and intact areas. The observed deterioration rate affirms inefficient hindrance to corrosion related processes, which are due to the low zinc content and the high PCAIP caused decreased galvanic efficiency of the primer. With lower amount of the nano-size inhibitor particles, the **H2** showed real improvement in the active function compared to the **H1** and **ZA** which is reflected by the low intensity rust formation and the very progress in the migration front of delaminated areas around scribes. Repeated test results of the **H3** pointed out advanced protection ability of such hybrid formulation against delamination and prevention of iron rust formation. Starting degradation of the coating only in the later stage also suggest increased protection functionality. As a result of optimal hybrid formulation besides the incorporation of high amount of zinc pigment, the **H4** afforded excellent protection performance against rust formation and coating delamination. Only very low scale blistering was detected over intact areas. These characteristics are attributed to the high zinc PVC and the low PCAIP contents ensured low porosity and electrolytic conductivity as well as the high utilisation efficacy of anodic current for steel protection. Robust protection nature of the coating is not only emphasised by the almost uniform extent of small scale corrosion around the scribes and lower intensity of steel rusting but the later initiation of coating deterioration and the very low migration progress of delamination fronts. The even higher zinc content combined with less PCAIPs resulted in worsened active protection capability of the **H5** which is noted by the greater rate of rust formation around scratches and the pronounced extent of delamination over the buried surface. Only the low blistering susceptibility of the coating was similar to the massive

performance providing **H4**. Nevertheless, the overall deterioration of the **H5** was greater started in the early stage of the test compared to the **H4**.

To conclude about the protection function of the various zinc-rich hybrid compositions, the following considerations are to be taken into account. The paint mixture is assumed to be composed of randomly distributed hard spheroids of zinc pigments and the inhibitor particles with average size of 3 μm and 30 nm, respectively. Hence, the extent of interface between the organic vehicle and the zinc pigments defines bulk and interfacial density of the inhibitor particles in the epoxy at a given PCAIP content. Once it was defined for polymeric composites, for electrical percolation theoretical interparticle distance must be lower than 10 nm as a gap width based on electron tunnelling mechanism [52,53]. Based on our experiments, the most viable long-term protection was noticed to the 80 wt.% zinc contained hybrid formulation. Ignoring the effects of solvation based swelling, unbundling and bridging aggregation of the partially restricted mobility featuring PPy segments, also the possible settling of the particles, higher distance must be valid between adjacent PCAIPs in all hybrid paints than it would be considered to assure electrical percolation between zinc pigments. On the other hand, around ~5−8% of the zinc surface area is estimated to interact with PCAIPs within 10 nm distance volume range in the vicinity of the grains. In fact, despite the low concentration of the PCAIPs such particles are able to afford valuable anodic protection to metallic surfaces [54]. On the other hand, the low PPy contents (and the nano-size alumina) provide low density paths across epoxy of the hybrids entailing in hindered permeation of the electrolyte. Hence, zinc corrosion should only be low scale activated by the infiltrating solution and inhibited somewhat by the PCAIPs in case of their statistical even distribution, despite the firm corrosion prevention ability of PPy according to the literature data [56,57]. Thus, moderate galvanic function of the hybrids must take benefit from the moderately interacting and low spatial density of the PCAIPs besides low porosity of the primers, leading to appropriate media for suppressed rate of zinc corrosion at the same time. Experimental results disclosing the absence of cathodic delamination failure and the various scales of accumulation of cationic species both in the primers and near the steel surface corroborate low but efficient galvanic function of the hybrids. Otherwise, major part of the PCAIPs was highly dispersed in the size range of about 20 nm but not evenly distributed in the epoxy (as it was impressed by TEM observations), facilitating the electrical percolation of the hybrids relaying on infinite percolating cluster formation (smoothly graded interface and well interconnected 3D structure of the dispersed phase). Our calculations suggest that inhibitor particles with diameter of 10 nm would contribute effectively to the electrical conductivity of the low zinc PVC type hybrid coatings. This is in agreement with the aspects of double and multiple percolation theory [57,58] describing the relationship of decreasing size of electrically conducting particles and percolation thresholds of the composites. Such behaviour was recognised even for the **H1** and **H2** samples containing isotropic zinc grains at 60 wt.%, which primers should not support sacrificial type anodic current based corrosion prevention without other electrically conducting or semi-conducting components. Average density of the nano-size PCAIPs ($\sim 2\times10^{20}$ m^{-3}) allows hindering the electrolyte ingress into the coatings. This behaviour of the particles is in line with the nano-particle impact on composites [17], despite the permeability of PPy and the hydrated alumina. Further estimation suggests that hybrid primers with 70 wt.% zinc content and the applied amount of the PCAIPs would feature static dissipative electrical conductivity with the specific resistance of about $R\approx1\times10^{4}$–1×10^{11} Ω. On the other hand, the three-dimensionally moderately interlinked semi-conducting PCAIPs affecting the intensity of sacrificial anodic current, the overall corrosion prevention mechanism may probably involve partial p-n junction regulation in the hybrids as a result of piled n- and p-type semiconductors of the evolving zinc oxide and PPy, corresponding to

Patil, et al. [59]. This function is surmised to lead to partially improved protection performance with the mechanism of semiconductor incorporated sacrificial metallic pigments based systems proposed by R.N. Jagtap, et al. [8].

5. Conclusion

With the aim of seeking optimal hybrid primer formulation based on the mixture of PPy coated alumina type inhibitor particles and zinc pigments besides gaining knowledge over the corrosion protection mechanism, the following conclusions are to be drawn.

Optimal corrosion preventive action of the hybrid paints involves low intensity but efficient galvanic function and firm barrier behaviour along with the decreased accumulation rate of precipitated corrosion products and leaching of dissolved species. As a result, all the terms of improved electrical and lower electrolytic conductivity as well as corrosion inhibition of the zinc pigments besides the mitigated oxidative degradation of the epoxy vehicle were exploited to avoid the phenomenon of blistering and cathodic delamination type cohesion and adhesion failure over long-term corrosion tests. Advanced protection performance was obtained by one preferred hybrid formulation comprising zinc pigments and PCAIPs at 80 and 1.75 wt.% despite the suggestion of hard spheroids based theory with the lack of enough electrical percolation affecting the efficiency of galvanic function. Therefore, major part of the highly dispersed PCAIPs is surmised to have been swollen and partially unbundled causing small scale bridging as well as inhomogeneously distributed around the bulky zinc pigments. Thus, electrical percolation of the zinc-rich primers and corrosion inhibition of the sacrificial zinc pigments must be facilitated by the interaction with the low density of the semi-conductive inhibitor particles.

Acknowledgement

This work was partially carried out as part of the TÁMOP-4.2.1.B-10/2/KONV-2010-0001 project in the framework of the New Hungarian Development Plan. The realization of this project is supported by the European Union, co-financed by the European Social Fund. Thanks are due to Zoltán Klencsár for the Mössbauer spectroscopy measurements. Ágnes Stahl is honoured for her consultancy. Authors are indebted to the Hungarian paint industry partner: Egrokorr, for the chemicals provided and practical advice. Authors are grateful for the helpful discussions provided by Abdul Shaban, Felhősi Ilona, Mihály Judith and Nyikos Lajos.

References

[1] S. Shreepathi, P. Bajaj, B.P. Mallik, Electrochim. Acta 55 (2010) 5129–5134.
[2] C.A. Gervasi, A.R. Di Sarli, E. Cavalcanti, O. Ferraz, E.C. Ducharsky, S.G. Real, J.R. Vilche, Corros. Sci. 36 (1994) 1963–1972.
[3] V. Zivica, Bull. Mater. Sci. 25 (2002) 371–373.
[4] O. Øystein Knudsen, U. Steinsmo, M. Bjordal, Prog. Org. Coat. 54 (2005) 224–229.
[5] M.T. Rodríguez, J.J. Gracenea, J.J. Saura, J.J. Suay, Prog. Org. Coat. 50 (2004) 68–74.
[6] J.R. Vilche, E.C. Bucharsky, C.A. Giudice, Corros. Sci. 44 (2002) 1287–1309.
[7] R.N. Jagtap, R. Nambiar, S.Z. Hassan, V.C. Malshe, Prog. Org. Coat. 58 (2007) 253–258.
[8] R.N. Jagtap, P.P. Patil, S.Z. Hassan, Prog. Org. Coat. 63 (2008) 389–394.
[9] T. Tüken, B. Yazici, M. Erbil, Mater. Chem. Phys. 99 (2006) 459–464.
[10] S.K. Geer, T.R. Hawkins, US patent 7595009, 2009.
[11] E. Armelin, M. Martí, F. Liesa, J.I. Iribarren, C. Alemán, Prog. Org. Coat. 69 (2010) 26–30.
[12] A. Meroufel, C. Deslouis, S. Touzain, Electrochim. Acta 53 (2008) 2331–2338.
[13] M. Tiitu, A. Talo, O. Forsén, O. Ikkal, Polymer 46 (2005) 6855–6861.

[14] R. Partch, S.G. Gangolly, E. Matijevic, W. Cai, S. Arajs, J. Colloid Interface Sci. 144 (1991) 27–35.
[15] S. Maeda, S.P. Armes, J. Mater. Chem. 4 (1994) 935–942.
[16] F.M. Huijs, F.F. Vercauteren, B. de Ruiter, D. Kalicharan, G. Hadziioannou, Synth. Met. 102 (1999) 1151–1152.
[17] R.N. Rothon, Adv. Polym. Sci. 139 (1999) 67–107.
[18] D.R. Paul, L.M. Robeson, Polymer 49 (2008) 3187–3204.
[19] H. Chriswanto, H. Ge, G.G. Wallace, Chromatographia 37 (1993) 423–428.
[20] A. Malinauskas, Polymer 42 (2001) 3957–3972.
[21] M. Ionita, A. Pruna, Prog. Org. Coat. 72 (2011) 647–652.
[22] J.I. Martins, T.C. Reis, M. Bazzaoui, E.A. Bazzaoui, L. Martins, Corros. Sci. 46 (2004) 2361–2381.
[23] J. Bonastre, P. Garcés, F. Huerta, C. Quijada, L.G. Andión, F. Cases, Corros. Sci. 48 (2006) 1122–1136.
[24] P. Ocón, A. B. Cristobal, P. Herrasti, E. Fatas, Corros. Sci. 47 (2005) 649–662.
[25] S.C. Yang, W. Li, US Patent 6803446, 2004.
[26] D.E. Tallman, K.L. Levine, C. Siripirom, V.G. Gelling, G.P. Bierwagen, S.G. Croll Appl. Surf. Sci. 254 (2008) 5452–5459.
[27] A. Gergely, É. Pfeifer, I. Bertóti, T. Török, E. Kálmán, Corros. Sci. 53 (2011) 3486–3499.
[28] E. Akbarinezhad, F. Rezaei, J. Neshati, Prog. Org. Coat. 61 (2008) 45–52.
[29] J.F. Moulder W.F. Stickle, P.E. Sobol, K.D. Bomben, Handbook of X-Ray Photoelectron Spectroscopy, Perkin-Elmer Corp., Eden Prairie, Minnesota, 1992.
[30] NIST Database: http://srdata.nist.gov/xps/
[31] F. Nagy, Z. Klencsár, Nucl. Instrum. Methods B 245 (2006) 528–538.
[32] Z. Klencsár, E. Kuzmann, A. Vértes, J. Radioanal. Nucl. Chem. 210 (1996) 105–118.
[33] M.M. Ayad, J. Mater. Sci. Lett. 22 (2003) 1577–1579.
[34] G. Goncalves, E. Fortunato, J. Martins, R. Martins, Mater. Sci. For. 514-516 (2006) 43–47.
[35] Y. Tian, F. Yang, W. Yang, Synth. Met. 156 (2006) 1052–1056.
[36] G. Socrates, Infrared and Raman Characteristic Group Frequencies, John Wiley & Sons, Ltd. Baffins Lane, Chichester, England, 2001.
[37] M. Omastova, M. Trchova, J. Kovarova, J. Stejskal, Synth. Met. 138 (2002) 447–455.
[38] L. Liu, Ch. Zhao, Y. Zhao, N. Jia, Q. Zhou, M. Yan, Z. Jiang, Europ. Polym. J. 41 (2005) 2117–2121.
[39] G. Cho, D.T. Glatzhofer, B.M. Fung, W.-L. Yuan, E.A. O'Rear, Langmuir 16 (2000) 4424–4429.
[40] C. M. Hansen, Hansen solubility parameters: a user's handbook CRC Press, 2007, ISBN 0849372488.
[41] P.A. Sorensen, K. Dam-Johansen, C.E. Einell, S. Kill, Prog. Org. Coat. 68 (2010) 283–292.
[42] T. Nguyen, J.B. Hubbard, J.M. Pommersheim, J. Coat. Technol. 68 (1996) 45–56.
[43] M.J. Pourbaix, Atlas d'équilibres électrochimiques. Gauthier-Villars, Paris, 1963.
[44] W. Fürbeth, M. Stratmann, Corros. Sci. 43 (2001) 229–241.
[45] M.N. Ismail, M.S. Ibrahim, M.A.A. El-Ghaffar, Polym. Degrad. Stab. 62 (1998) 337–341.
[46] O. Inganäs, R. Erlandsson, C. Nylander, I. Lundström, J. Phys. Chem. Solids 45 (1984) 427–432.
[47] J. Mostany, B.R. Scharifker, Electrochim. Acta 42 (1997) 291–301.
[48] H. Xie, M. Yan, Z. Jiang, Electrochim. Acta 42 (1997) 2361–2367.
[49] D.L.A. de Faria, V. Silva, M.T. de Oliveira, J. Raman Spec. 28 (1997) 873–878.
[50] M. Bouchard, D.C. Smith, Spectrochim. Acta A. 59 (2003) 2247–2266.
[51] R.M. Taylor, Clays Clay Miner. 32 (1984) 167–174.
[52] G.R. Fiuschau, S. Yoshikawa, R.E. Newnham. J. Appl. Phys. 72 (1992) 953–959.
[53] R.D. Sherman, L.M. Middleman, S.M. Jacobs, Polym. Eng. Sci. 23 (1983) 36–46.
[54] A. Gergely, Z. Pászti, O. Hakkel, E. Drotár, J. Mihály, E. Kálmán, Mater. Sci. Engineer. B http://dx.doi.org/10.1016/j.mseb.2012.03.049
[55] S.A. Kumar, K.S. Meenakshi, T.S.N. Sankaranarayanan, S. Srikanth, Prog. Org. Coat. 62 (2008) 285–292.
[56] M. Bazzaoui, J.I. Martins, S.C. Costa, E.A. Bazzaoui, T.C. Reis, L. Martins, Electrochim. Acta 51 (2006) 2417–2426.
[57] X. Jing, W. Zhao, L. Lan, J. Mater. Sci. Lett. 19 (2000) 377–379.
[58] K. Levon, A. Margolina, A.Z. Patashinsky, Macromolecules 26 (1993) 4061–4063.
[59] R.C. Patil, S. Radhakrishnan, Prog. Org. Coat. 57 (2006) 332–336.

Figure captions:

Fig. 1. TEM images of the polypyrrole deposited alumina particles.

Fig. 2. FTIR spectra of free-standing polypyrrole prepared in water (PPy1), aqueous ethanol solution (PPy2), and the polypyrrole deposited alumina particles.

Fig. 3. Rheology characterization of dissolved alkyd resin, alkyd dispersion of alumina and the PCAIPs at solid phase content of 3.846 wt.%, dynamic measurements: (a) frequency sweep at 1 Pa, (b) amplitude sweep at 1 Hz, (c) constant rate measurement with upward (uw.) and downward (dw) curves of shear stresses and strain rates, and (d) constant force measurement.

Fig. 4. Open-circuit potential (a) and the electrochemical impedance spectra (Bode plots) of steel substrates coated with (b) neat epoxy **E**, (c) traditional type zinc-rich **Z**, and (d) alumina consisting zinc-rich **ZA** paint coatings. Immersion tests with 1 M aqueous NaCl solution presented by time of exposure (in days).

Fig. 5. Open-circuit potential (a) and the electrochemical impedance spectra (Bode plots) of steel substrates coated with the PPy-deposited alumina particles comprising hybrid paint coatings containing zinc at (b) 60 in **H1**, (c) 60 in **H2**, (d) 70 in **H3**, (e) 80 in **H4,** and (f) 85 wt.% in **H5**. Immersion tests with 1 M aqueous NaCl solution presented by time of exposure (in days).

Fig. 6. Relative intensities of the elements in the cross-section of **ZA** detected by GD-OES: (a) before and (b) after the immersion test.

Fig. 7. Relative intensities of the elements in the cross-section of **H2** detected by GD-OES: (a) before and (b) after the immersion test.

Fig. 8. Relative intensities of the elements in the cross-section of **H3** detected by GD-OES: (a) before and (b) after the immersion test.

Fig. 9. XPS spectra: (a) Fe 2p and (b) Zn 2p regions detected on the surface of steel specimens coated with immersion tested paint coatings.

Fig. 10. Ratio of the steel surface-detected species derived from XPS quantification data.

Fig. 11. FT-Raman spectra (a) and Mössbauer spectrum (b) acquired from the steel surface coated with the immersion tested **H1** coating.

Fig. 12. Photographs of the traditional zinc-rich **Z**, nano-size alumina contained zinc-rich **ZA** and the PCAIP composited zinc-rich **H1**–**H5** hybrid paint coatings, salt-spray chamber tested with 1 M NaCl solution with Prohesion® for 142 days.

Fig. 13. Evaluation of the salt-spray chamber tested paint coating samples over the 142 days period. Quality estimation was performed according to the ISO 4628-1 guidelines, respecting both the terms of uniform deterioration and scattered defects. The standard defined corrosion rating from unchanged state with no detectable defects to severe, or intense change with dense pattern of defects rated from 0 to5 correspond with the hereby presented scale of 10 to 0 meaning no perceptible changes to severe deterioration with high density of defects.

Fig. 1.

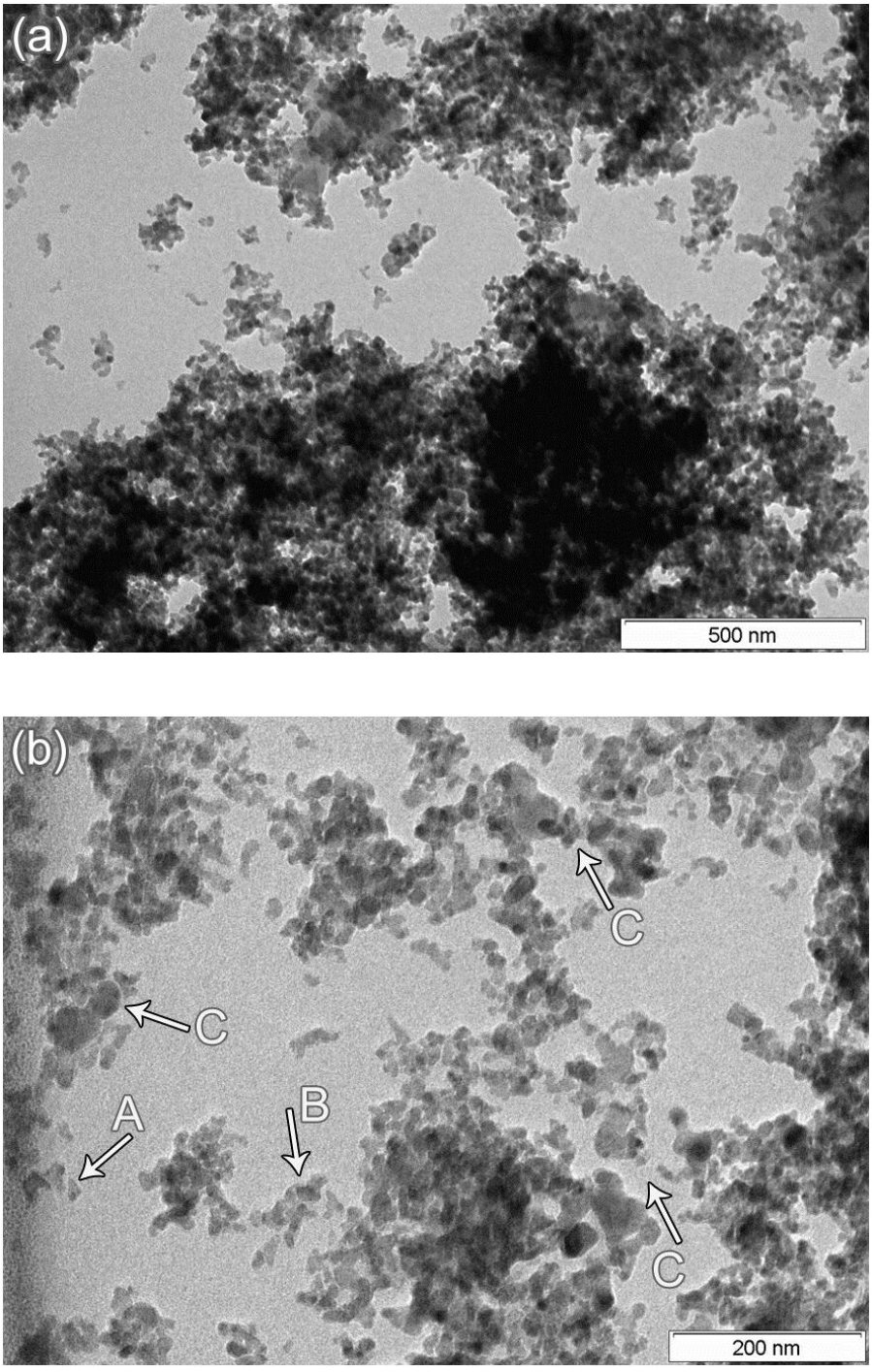

Fig. 2.

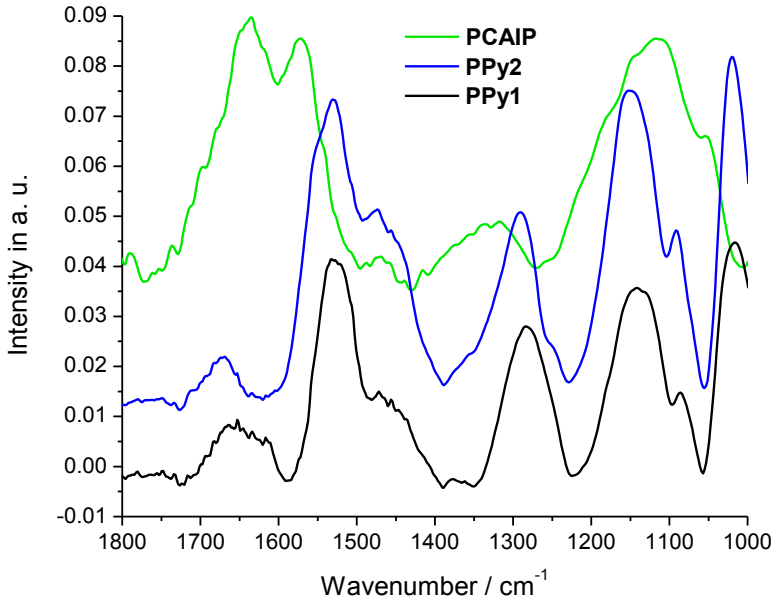
PCAlP
PPy2
PPy1
Intensity in a. u.
0.09
0.08
0.07
0.06
0.05
0.04
0.03
0.02
0.01
0.00
-0.01
1800
1700
1600
1500
1400
1300
1200
1100
1000
Wavenumber / cm-1

Fig. 3.

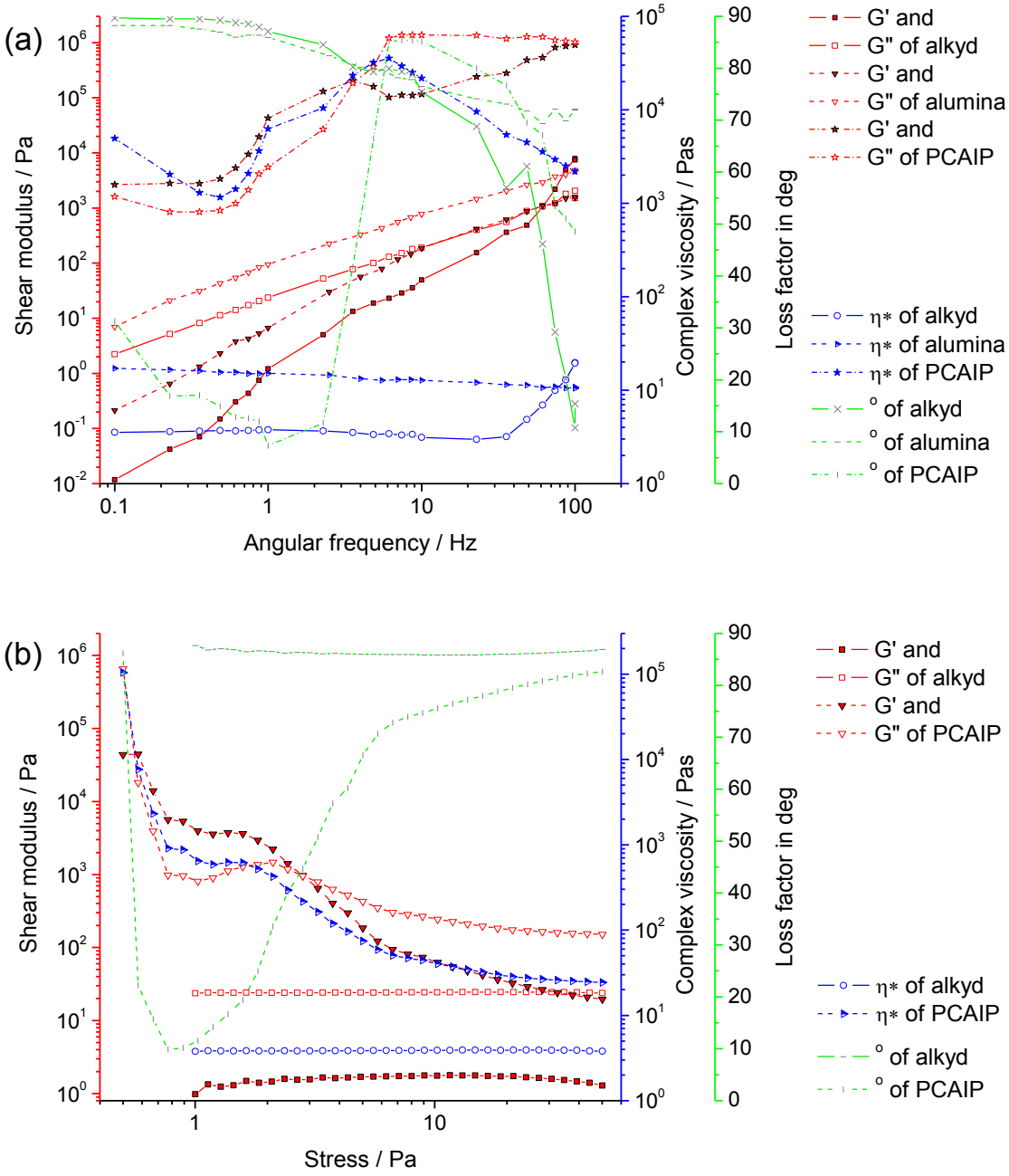
(a)
Shear modulus / Pa
Complex viscosity / Pas
Loss factor in deg
Angular frequency / Hz
G' and
G" of alkyd
G' and
G" of alumina
G' and
G" of PCAIP
η* of alkyd
η* of alumina
η* of PCAIP
° of alkyd
° of alumina
° of PCAIP
(b)
Shear modulus / Pa
Complex viscosity / Pas
Loss factor in deg
Stress / Pa
G' and
G" of alkyd
G' and
G" of PCAIP
η* of alkyd
η* of PCAIP
° of alkyd
° of PCAIP

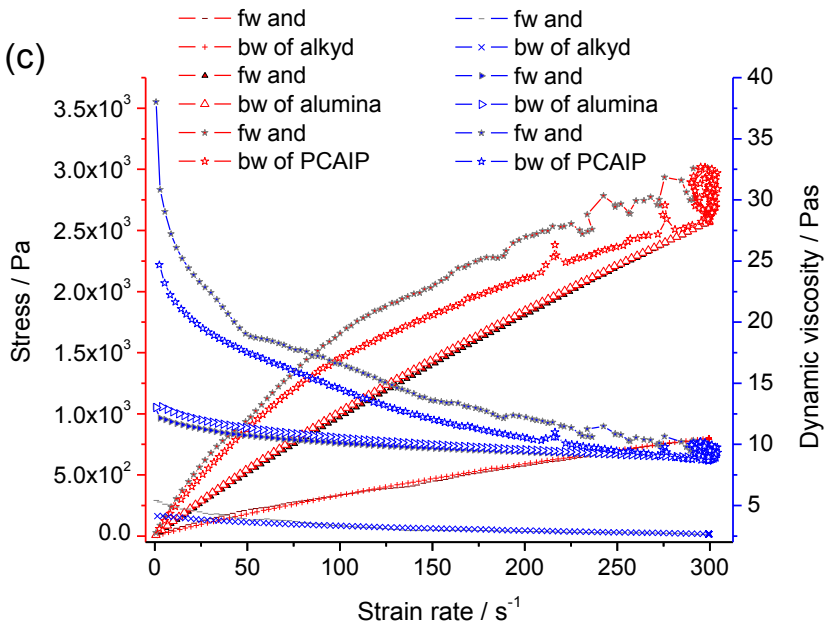
(c)
fw and
bw of alkyd
fw and
bw of alumina
fw and
bw of PCAIP
fw and
bw of alkyd
fw and
bw of alumina
fw and
bw of PCAIP
Stress / Pa
Dynamic viscosity / Pas
Strain rate / s-1

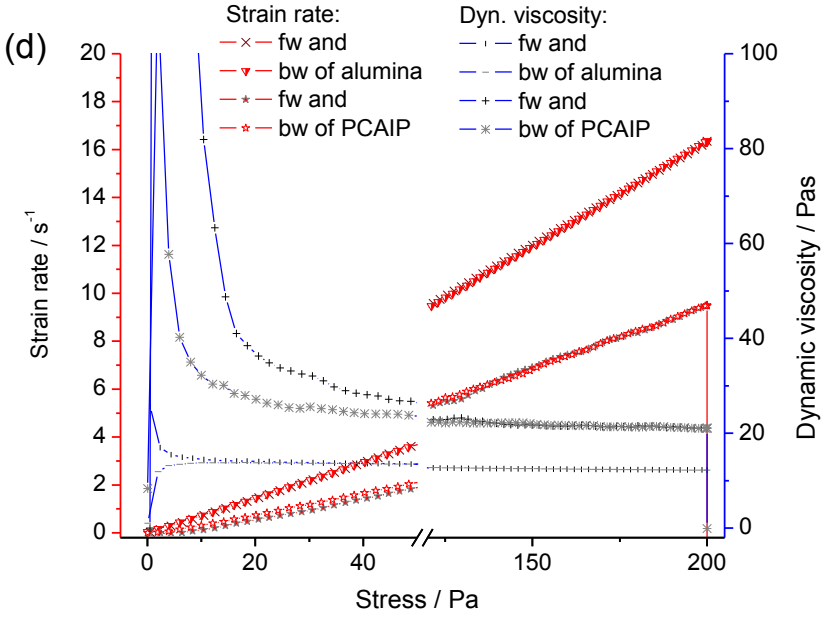
(d)
Strain rate:
fw and
bw of alumina
fw and
bw of PCAIP
Dyn. viscosity:
fw and
bw of alumina
fw and
bw of PCAIP
Strain rate / s-1
Dynamic viscosity / Pas
Stress / Pa

Fig. 4.

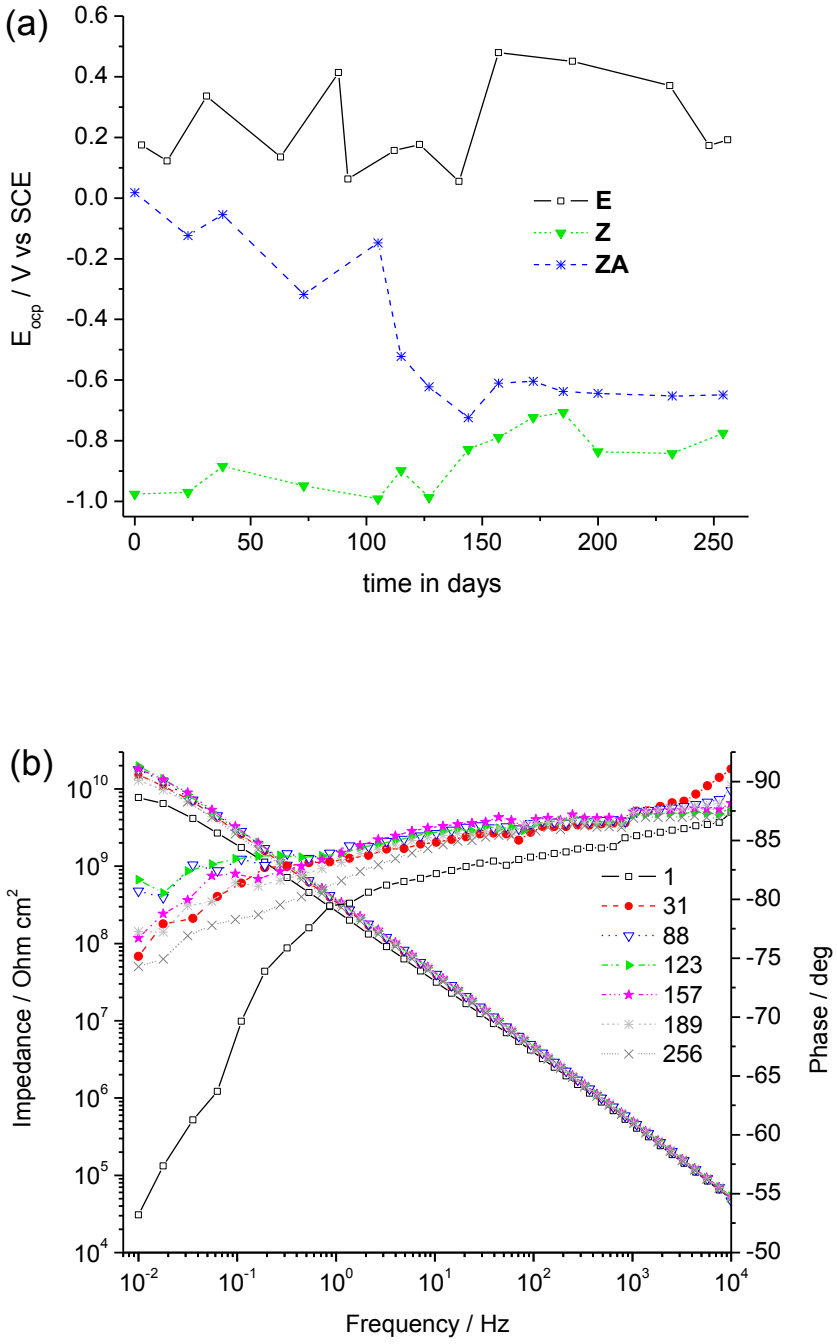
(a)
0.6
0.4
0.2
0.0
-0.2
-0.4
-0.6
-0.8
-1.0
E_ocp / V vs SCE
0
50
100
150
200
250
time in days
E
Z
ZA
(b)
10^10
10^9
10^8
10^7
10^6
10^5
10^4
Impedance / Ohm cm^2
10^-2
10^-1
10^0
10^1
10^2
10^3
10^4
Frequency / Hz
-90
-85
-80
-75
-70
-65
-60
-55
-50
Phase / deg
1
31
88
123
157
189
256

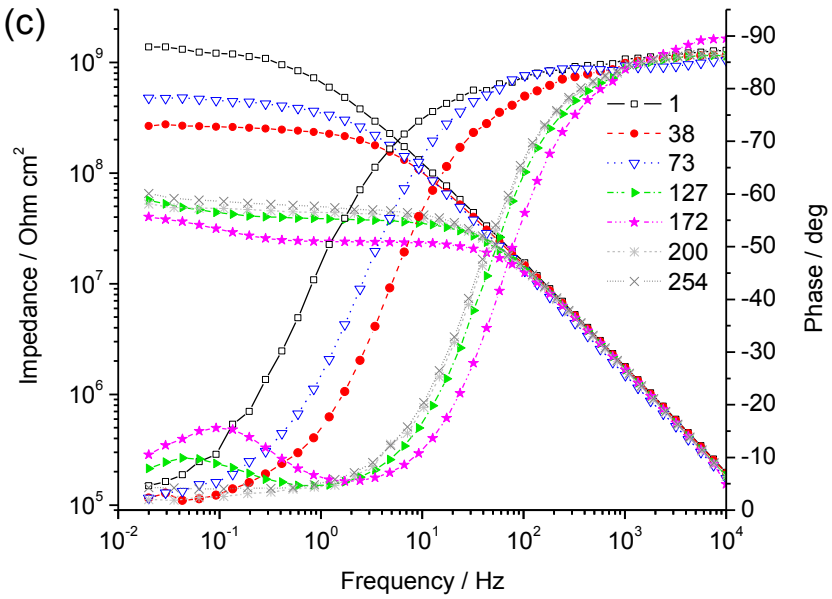
(c)
Impedance / Ohm cm^2
Phase / deg
Frequency / Hz
1
38
73
127
172
200
254

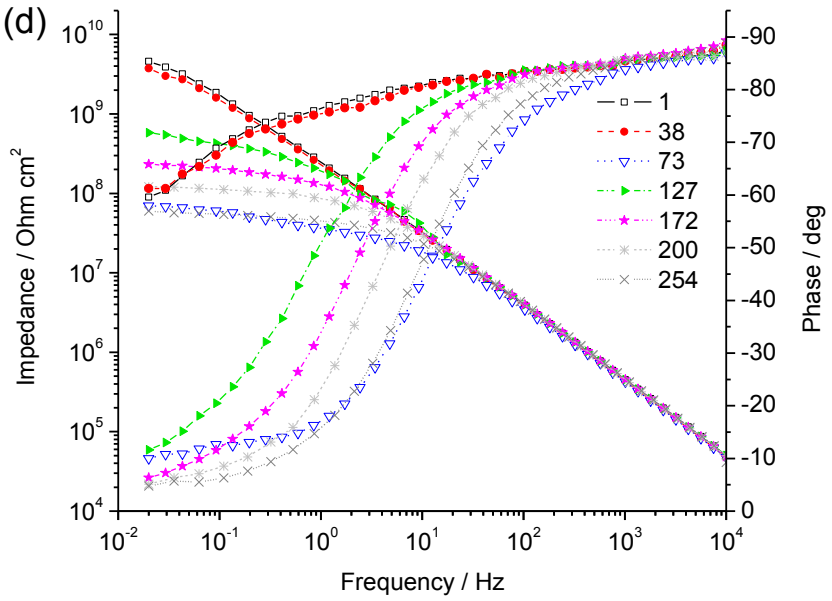
(d)
Impedance / Ohm cm^2
Phase / deg
Frequency / Hz
1
38
73
127
172
200
254

Fig. 5.

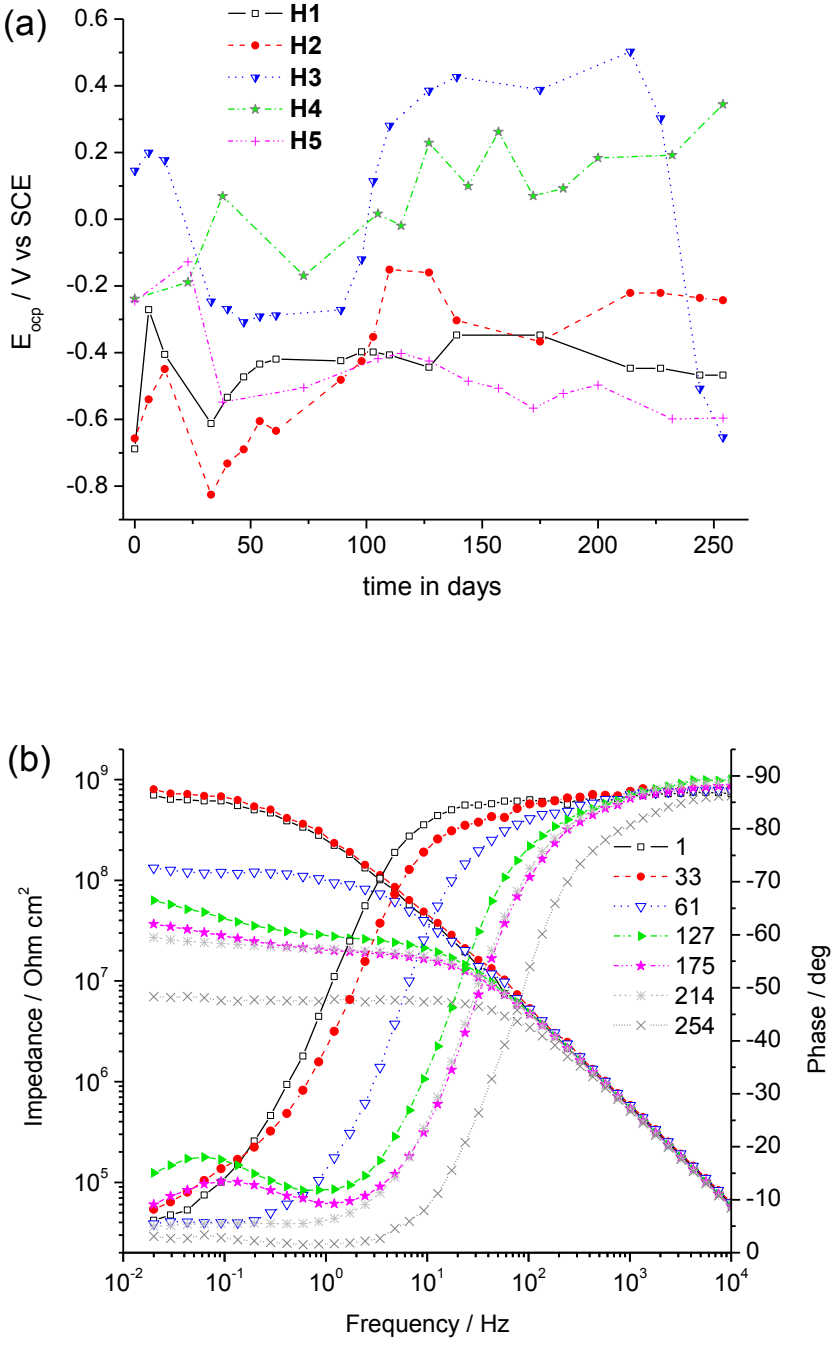
(a)
H1
H2
H3
H4
H5
E_{ocp} / V vs SCE
time in days
(b)
Impedance / Ohm cm^2
Phase / deg
Frequency / Hz
1
33
61
127
175
214
254

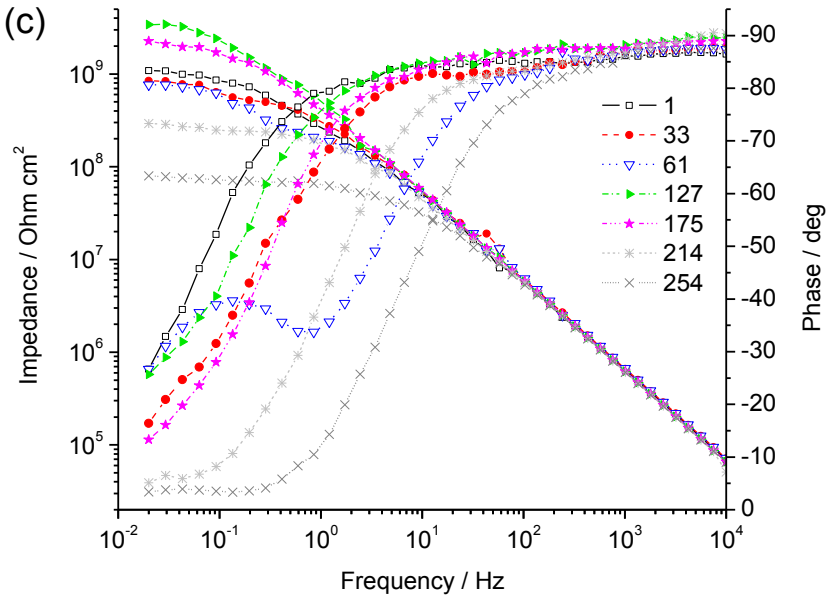
(c)
Impedance / Ohm cm^2
Phase / deg
Frequency / Hz
1
33
61
127
175
214
254

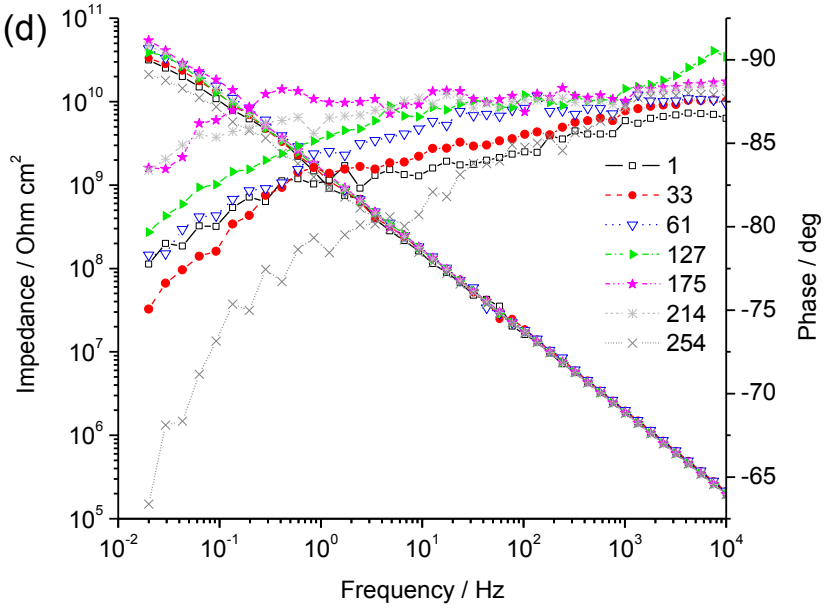
(d)
Impedance / Ohm cm^2
Phase / deg
Frequency / Hz
1
33
61
127
175
214
254

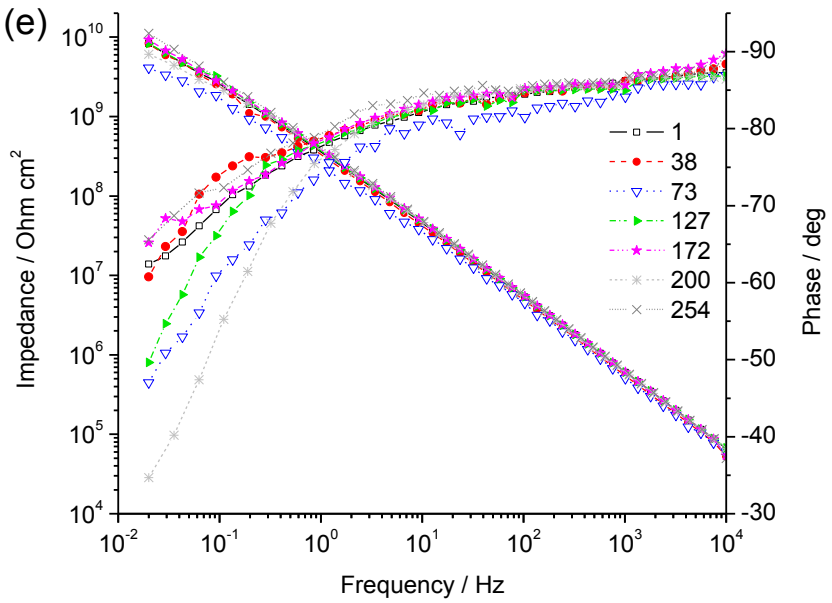
(e)
Impedance / Ohm cm^2
Phase / deg
Frequency / Hz
1
38
73
127
172
200
254

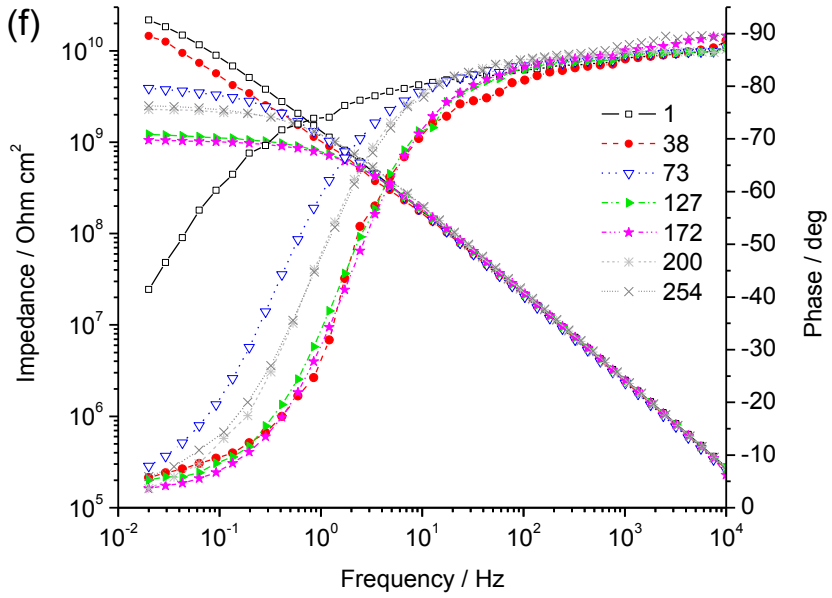
(f)
Impedance / Ohm cm^2
Phase / deg
Frequency / Hz
1
38
73
127
172
200
254

Fig. 6.

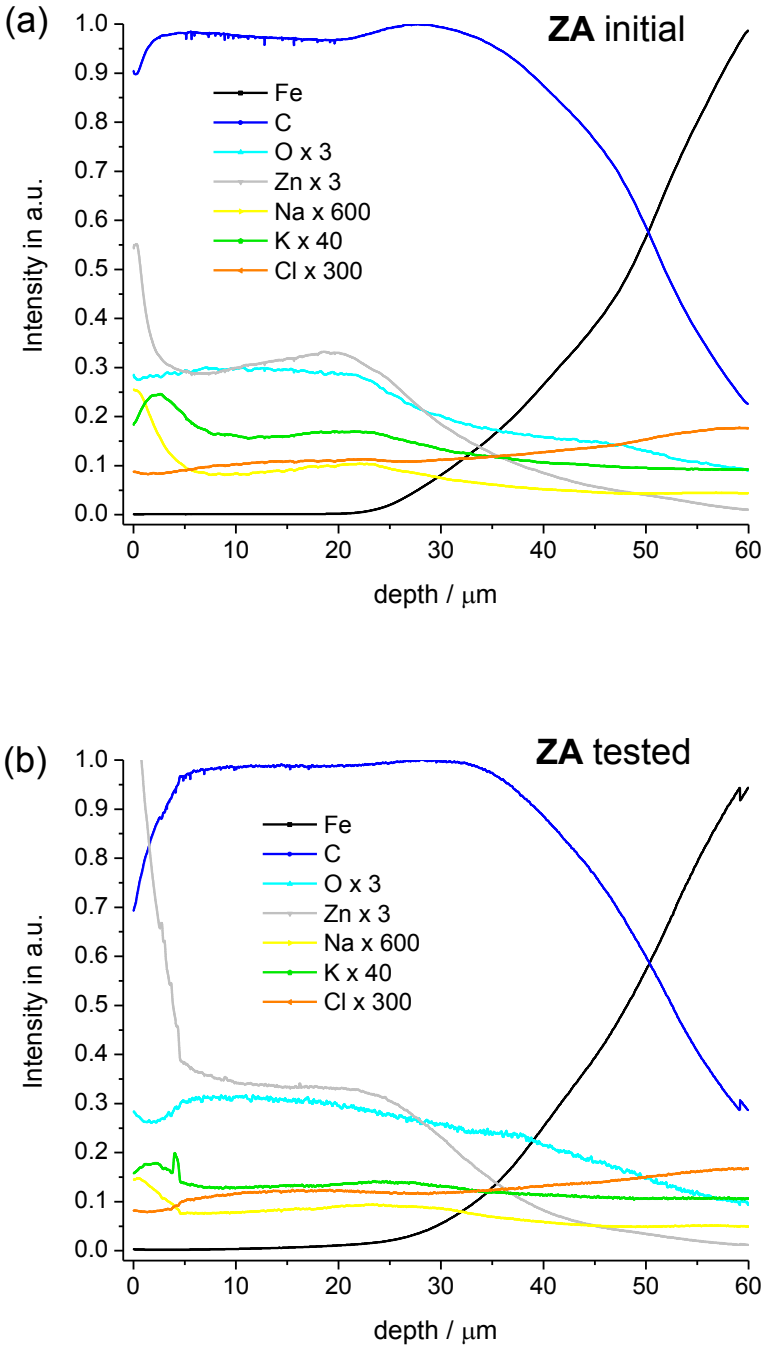
(a)
ZA initial
Fe
C
O x 3
Zn x 3
Na x 600
K x 40
Cl x 300
Intensity in a.u.
depth / μm
(b)
ZA tested
Fe
C
O x 3
Zn x 3
Na x 600
K x 40
Cl x 300
Intensity in a.u.
depth / μm

Fig. 7.

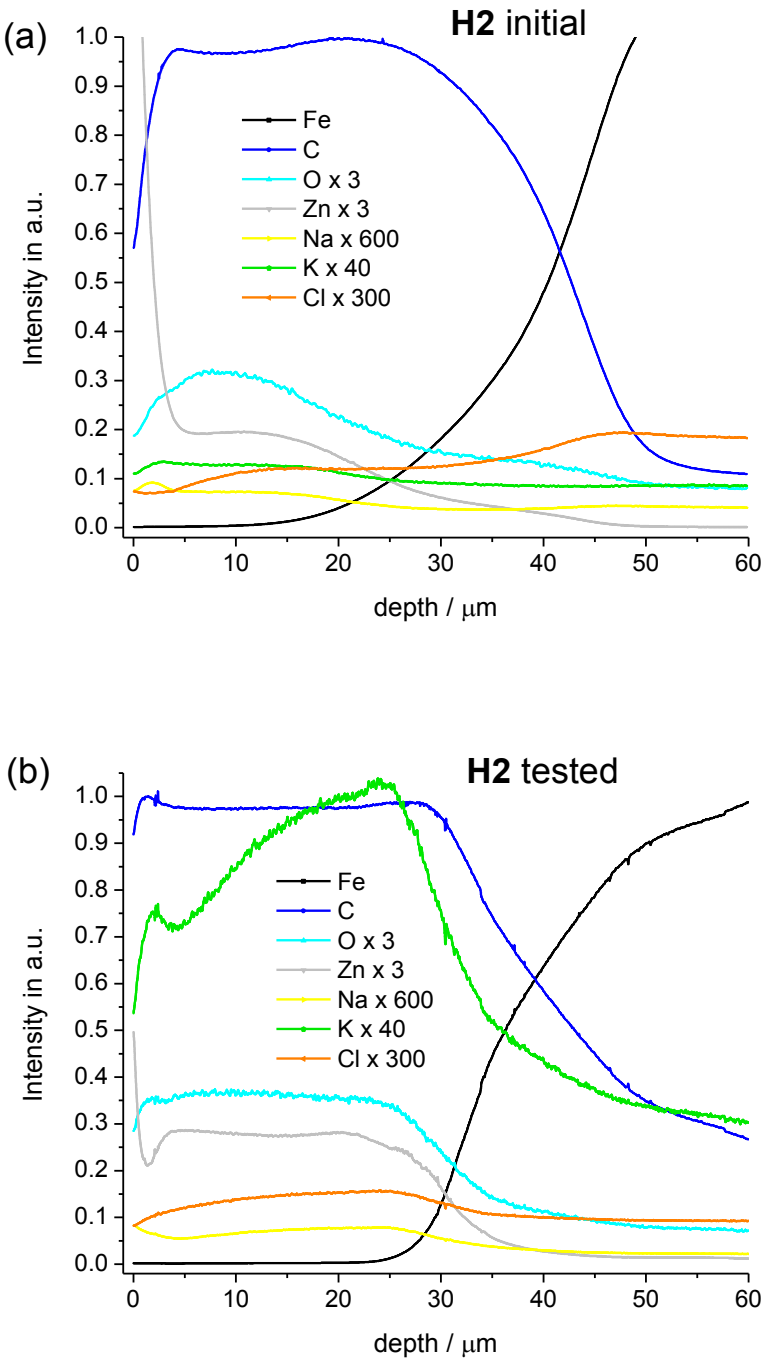
(a)
H2 initial
Intensity in a.u.
depth / μm
Fe
C
O x 3
Zn x 3
Na x 600
K x 40
Cl x 300
(b)
H2 tested
Intensity in a.u.
depth / μm
Fe
C
O x 3
Zn x 3
Na x 600
K x 40
Cl x 300

Fig. 8.

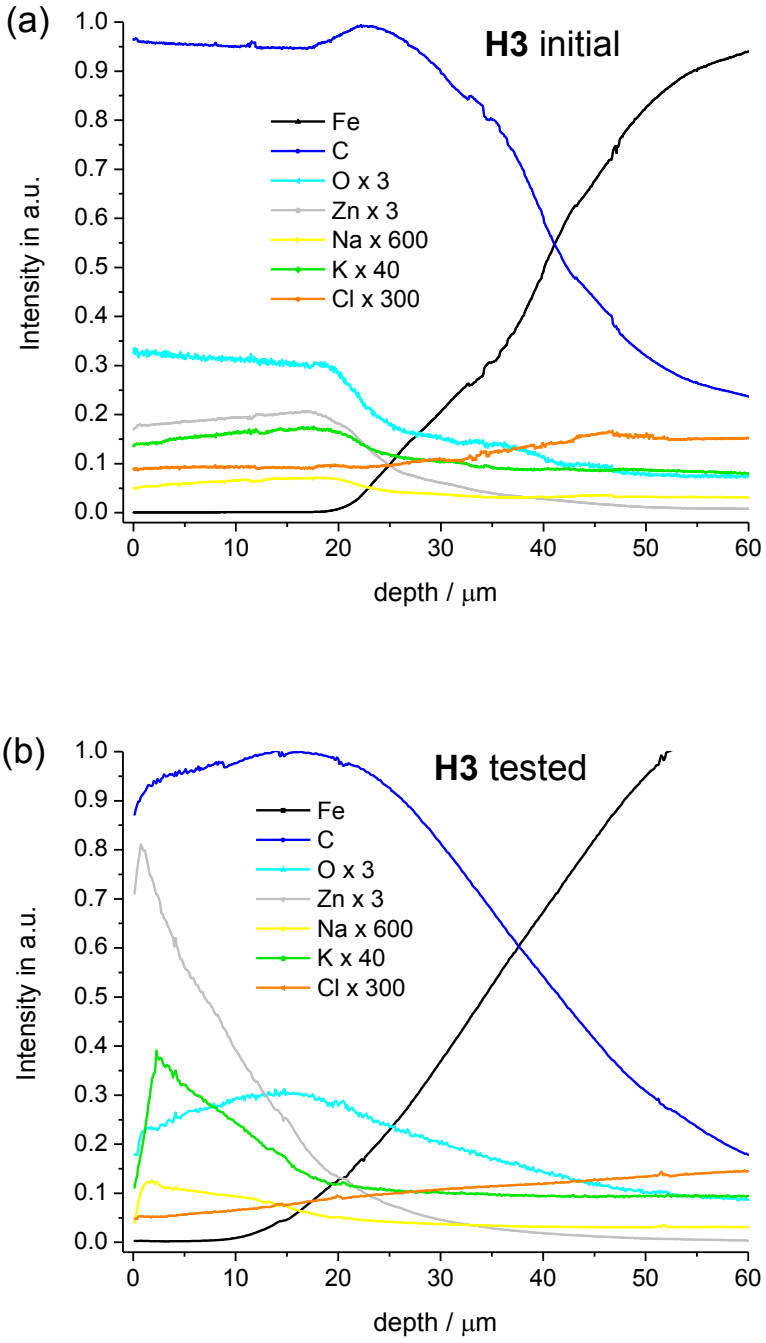
(a)
H3 initial
Fe
C
O x 3
Zn x 3
Na x 600
K x 40
Cl x 300
Intensity in a.u.
depth / μm
(b)
H3 tested
Fe
C
O x 3
Zn x 3
Na x 600
K x 40
Cl x 300
Intensity in a.u.
depth / μm

Fig. 9.

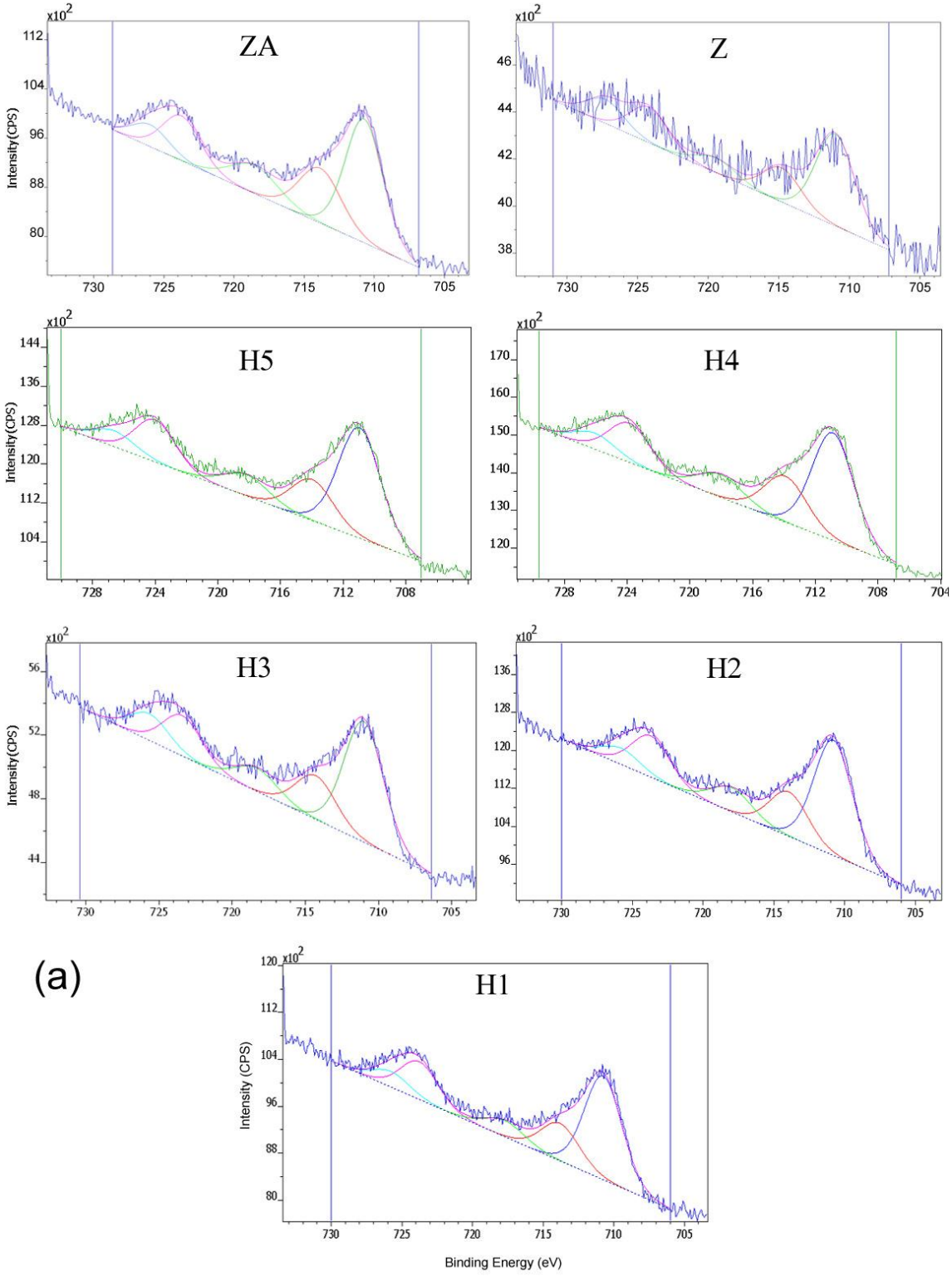
ZA
Z
H5
H4
H3
H2
H1
(a)
Intensity(CPS)
Intensity (CPS)
Binding Energy (eV)
x10^2

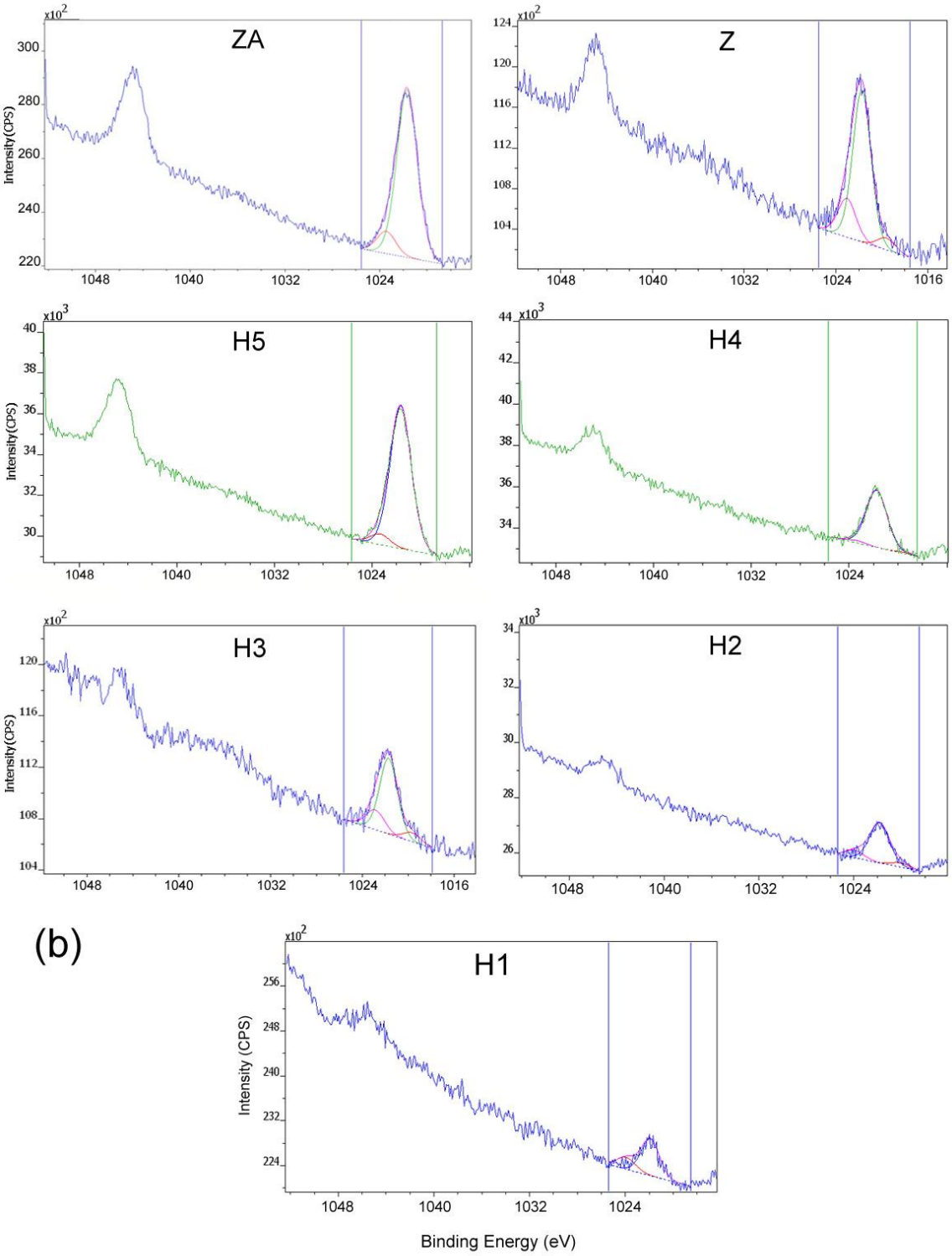
ZA
Z
H5
H4
H3
H2
H1
(b)
Intensity(CPS)
Intensity (CPS)
Binding Energy (eV)

Fig. 10.

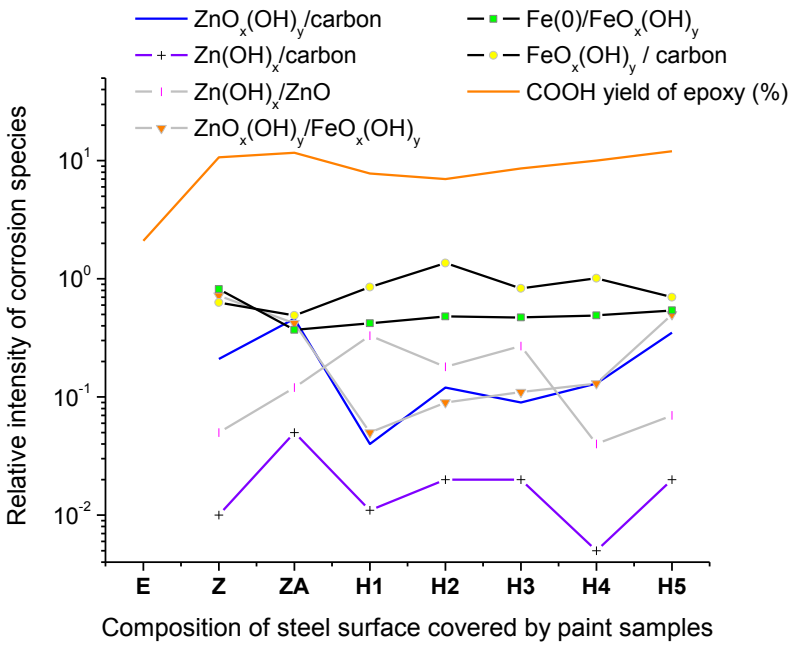
ZnO$_x$(OH)$_y$/carbon
Fe(0)/FeO$_x$(OH)$_y$
Zn(OH)$_x$/carbon
FeO$_x$(OH)$_y$ / carbon
Zn(OH)$_x$/ZnO
COOH yield of epoxy (%)
ZnO$_x$(OH)$_y$/FeO$_x$(OH)$_y$
Relative intensity of corrosion species
10^1
10^0
10^{-1}
10^{-2}
E
Z
ZA
H1
H2
H3
H4
H5
Composition of steel surface covered by paint samples

Fig. 11.

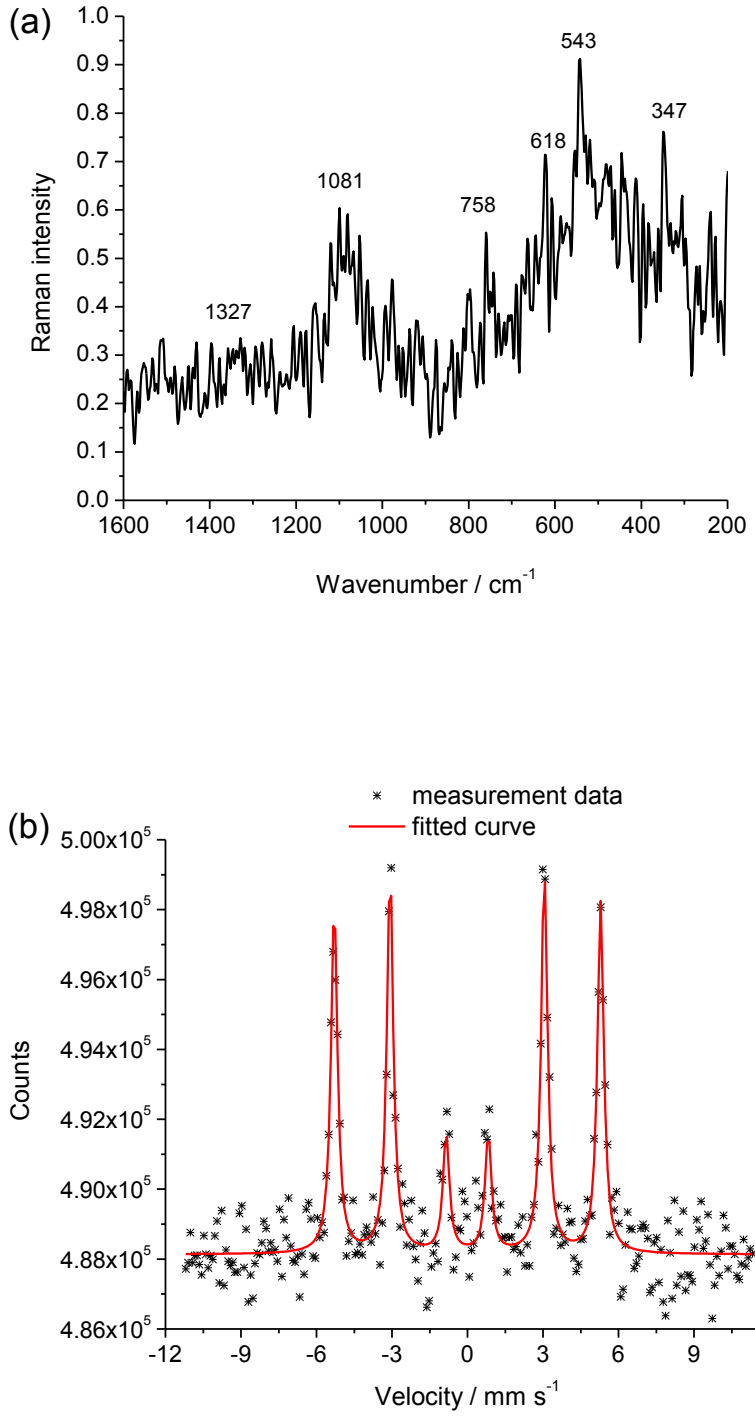
(a)
Raman intensity
Wavenumber / cm-1
1327
1081
758
618
543
347
(b)
measurement data
fitted curve
Counts
Velocity / mm s-1

Fig. 12.

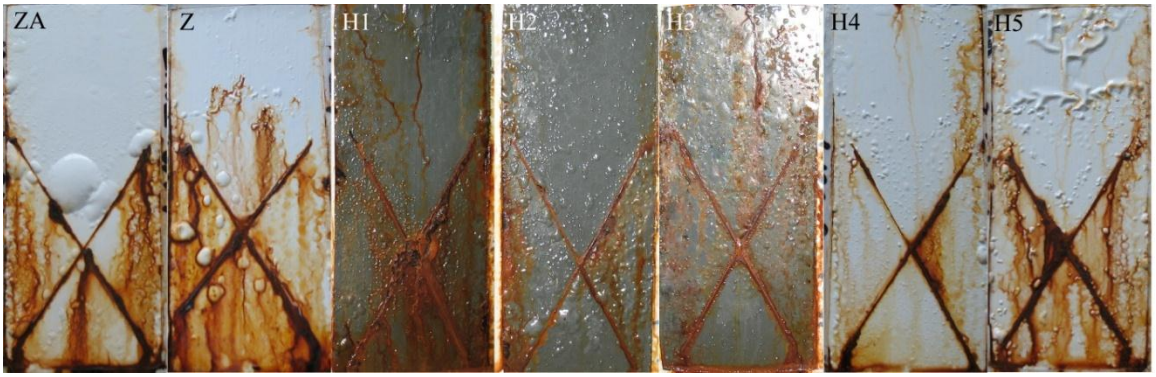
ZA
Z
H1
H2
H3
H4
H5

Fig. 13.

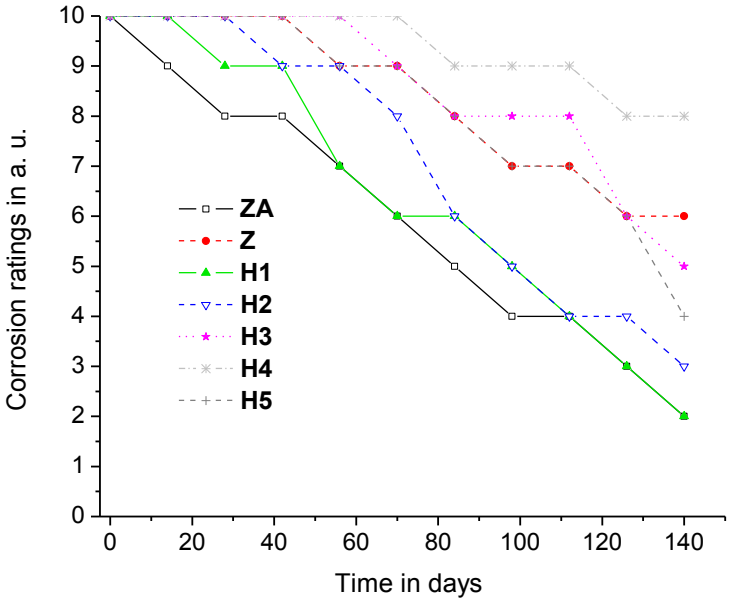
Corrosion ratings in a. u.
Time in days
ZA
Z
H1
H2
H3
H4
H5
0
1
2
3
4
5
6
7
8
9
10
0
20
40
60
80
100
120
140

Table captions:

Table 1

Zinc and the inhibitor particle contents of the cured primer and the epoxy resin of the paint coatings in weight percent (wt.%) and volume fraction (φ).

Table 2

Volume fraction (φ) of rheology investigated colloid dispersions of alumina and the PCAIPs in dissolved alkyd resin at solid contents of 3.846 wt.%. Thixotropy index and yield stress determined by constant rate and force mode measurements.

Table 3

Evaluation results of the immersion tested paint coatings corresponding to the EN ISO 4628:2005 standard with designation of degree of blistering (2) and delamination (8).

Table 4

Corrosion protection performance evaluation of the salt-spray chamber tested paint coatings, corresponding to the EN ISO 4628:2005 standard regarding the degree of blistering (2), rusting (3) and delamination (8).

Table 1

Coatings	PCAIP in the coating (wt.%)	PCAIP in the epoxy binder (wt.%)	PPy in the coating (φ)	PPy in the epoxy binder (φ)	Zinc (φ)
E	-	-	-	-	-
ZA	-	-	-	-	70 (26.8)
Z	-	-	-	-	90 (55.8)
H1	4.55	11.4	0.151 (3.28×10^{-3})	0.377 (4.02×10^{-3})	60 (18.3)
H2	3.67	9.3	0.121 (2.61×10^{-3})	0.308 (3.22×10^{-3})	60 (18.1)
H3	3.21	11.0	0.107 (2.81×10^{-3})	0.364 (3.89×10^{-3})	70 (25.8)
H4	1.75	9.1	0.060 (1.94×10^{-3})	0.301 (3.15×10^{-3})	80 (37.0)
H5	0.85	6.3	0.027 (1.07×10^{-3})	0.207 (2.14×10^{-3})	85 (45.0)

Table 2

Particles	Alumina (φ)	PPy (φ)	Thixotropy (Pa s^{-1})	σ (Pa)
alumina	1.670×10^{-2}	-	1535	1.4
PCAIP	1.616×10^{-2}	1.25×10^{-3}	79907	14.5

Table 3

Coatings	Degree of blistering size and density		Degree of delamination	Deadhesion of coatings
E	1	1 (less than few)	Complete	Homogeneous
ZA	2	4 (medium-dense)	Moderate	Homogeneous
Z	2	2 (few)	Considerabe	Inhomogeneous
H1	-	0 (none)	Complete	Homogeneous
H2	-	0 (none)	None	-
H3	-	0 (none)	None	-
H4	-	0 (none)	Complete	Homogeneous
H5	2	2 (few)	Complete	Homogeneous

Table 4

Coatings	Degree of blistering size and density		Degree (Ri) and area (%) of rusting over intact surface	Corrosion grade and delamination around scribes
ZA	2	2 (few)	Ri 2, 0.5	Grade 3 – severe
Z	3	2 (few)	Ri 3, 1	Grade 3 – slight
H1	2	4 (medium-dense)	Ri 3, 1	Grade 4 – moderate
H2	3	4 (medium-dense)	Ri 3, 1	Grade 2 – slight
H3	3	3 (medium)	Ri 3, 1	Grade 2 – slight
H4	2	3 (medium)	Ri 2, 0.5	Grade 2 – very slight
H5	3	3 (medium)	Ri 3, 1	Grade 3 – slight